CANCER

A potent CBP/p300-Snail interaction inhibitor suppresses tumor growth and metastasis in wild-type p53-expressing cancer

Hong-Mei Li[1]*, Yan-Ran Bi[1]*, Yang Li[1]*, Rong Fu[1]*, Wen-Cong Lv[1], Nan Jiang[1], Ying Xu[1], Bo-Xue Ren[1], Ya-Dong Chen[2], Hui Xie[3], Shui Wang[3], Tao Lu[2†], Zhao-Qiu Wu[1†]

The zinc finger transcription factor Snail is aberrantly activated in many human cancers and associated with poor prognosis. Therefore, targeting Snail is expected to exert therapeutic benefit in patients with cancer. However, Snail has traditionally been considered "undruggable," and no effective pharmacological inhibitors have been identified. Here, we found a small-molecule compound CYD19 that forms a high-affinity interaction with the evolutionarily conserved arginine-174 pocket of Snail protein. In aggressive cancer cells, CYD19 binds to Snail and thus disrupts Snail's interaction with CREB-binding protein (CBP)/p300, which consequently impairs CBP/p300-mediated Snail acetylation and then promotes its degradation through the ubiquitin-proteasome pathway. Moreover, CYD19 restores Snail-dependent repression of wild-type p53, thus reducing tumor growth and survival in vitro and in vivo. In addition, CYD19 reverses Snail-mediated epithelial-mesenchymal transition (EMT) and impairs EMT-associated tumor invasion and metastasis. Our findings demonstrate that pharmacologically targeting Snail by CYD19 may exert potent therapeutic effects in patients with cancer.

INTRODUCTION

Metastasis is the major cause of cancer motility and accounts for about 90% of cancer-associated death (1). Cancer metastasis is a multistep and inefficient process in which tumor cells disseminate from the primary tumors, survive in the circulation, and settle and grow at the distant vital organs (2–4). One key event of metastasis is the epithelial-mesenchymal transition (EMT), a highly conserved developmental program that enables cancer cells to acquire malignancy-associated traits and the properties of tumor-initiating cells (TICs) [also known as cancer stem cells (CSCs)] during tumor initiation and progression (5–9). A hallmark of EMT is the loss of expression of the key epithelial cell-cell adhesion protein E-cadherin, and the expression levels of mesenchymal markers vimentin, fibronectin, and N-cadherin are also up-regulated in cancer cells undergoing EMT (10). While EMT therapeutics that efficiently reverse EMT and impair EMT-associated therapeutic resistance and tumor-initiating ability (i.e., stemness) are recently proven to be an effective therapeutic strategy for cancer treatment, the therapeutic target of these agents remains unclear (11, 12).

Snail is recognized as a major transcriptional factor that induces EMT by repressing E-cadherin protein (13, 14). Emerging evidence suggests that Snail has a substantially broader impact on tumor progression and metastasis. Following its overexpression in mammary epithelial cells, Snail promotes an EMT program and acquisition of tumor-initiating properties while enhancing tumor invasion, metastasis, tumorigenicity, and therapeutic resistance (9, 10, 15, 16). In addition, Snail accelerates tumor metastasis by suppressing host immune surveillance and inducing tumor microenvironment modulation

(17, 18). Snail is also known to promote cancer cell survival by enhancing resistance to apoptosis under the genotoxic stress condition (19). We recently found that Snail deletion stabilizes wild-type, but not mutant, p53 and identified Snail as a molecular bypass that suppresses the antiproliferative and proapoptotic effect executed by wild-type p53 in breast cancer (BrCa) (20). However, it remains largely elusive whether p53 signaling pathway actively participates in Snail-mediated EMT, stemness, migration, and metastasis in cancer cells.

Snail is aberrantly activated in many human cancers and strongly associated with poor prognosis (20–23). Many oncogenic signaling pathways, such as hypoxia/hypoxia-inducible factor–1α, transforming growth factor–β (TGFβ), epidermal growth factor (EGF), fibroblast growth factor–2, and Notch, are implicated in the regulation of *Snail* gene expression (8, 24). In many cases, the posttranslational modification actively participates in the regulation of Snail protein. For instance, glycogen synthase kinase 3β (GSK3β) and protein kinase D1 (PKD1) can phosphorylate Snail and promote its polyubiquitination and degradation by forming a complex with E3 ligases beta-transducin repeats-containing proteins (β-TrCP) and F-Box protein 11 (FBXO11), respectively (25–29). Another E3 ligase F-box and leucine-rich repeat protein 14 (Fbxl14), the human homolog of the partner of paired gene product in *Xenopus*, is also known to degrade Snail in a phosphorylation-independent manner (30, 31). On the other hand, histone acetyltransferases (HATs) such as adenosine 3′,5′-monophosphate response element–binding protein–binding protein (CBP) and p300 interact with Snail and acetylate Snail at lysine-146 (K146) and K187, which consequently reduces Snail ubiquitination and thus enhances its protein stability (18). Given the important role of Snail in driving cancer progression, targeting Snail may exert potent therapeutic benefit in patients with cancer. In the present study, we have successfully identified a small-molecule compound CYD19 as a potent CBP/p300-Snail protein-protein interaction inhibitor. We further demonstrate that CYD19 restores Snail-dependent repression of wild-type p53 and thus impairs tumor cell growth and survival in vitro and in vivo. In addition,

[1]State Key Laboratory of Natural Medicines, School of Basic Medicine and Clinical Pharmacy, China Pharmaceutical University, Nanjing 211198, China. [2]State Key Laboratory of Natural Medicines, Laboratory of Molecular Design and Drug Discovery, School of Science, China Pharmaceutical University, Nanjing 211198, China. [3]Division of Breast Oncology, The First Affiliated Hospital of Nanjing Medical University, Nanjing 210036, China.
*These authors contributed equally to this work.
†Corresponding author. Email: zqwu@cpu.edu.cn (Z.-Q.W.); lutao@cpu.edu.cn (T.L.)

CYD19 reverses Snail-mediated EMT in aggressive cancer cells and thus diminishes tumor invasion and metastasis. Our findings demonstrate that Snail protein is a druggable target and that pharmacologically targeting Snail by compound CYD19 may exert potent therapeutic effects in patients with locally advanced and metastatic cancer.

RESULTS

CYD19 forms a high-affinity binding with Snail protein

To identify small-molecule compounds having high-affinity binding with Snail, we performed a virtual ligand screening assay based on compound docking into the potential binding pocket of Snail (32). Using the FTMap, an online computational solvent mapping software for predicting the binding "hotspots" of a protein (http://ftmap.bu.edu/login.php), we identified the evolutionarily conserved arginine-174 (R174) pocket (in red) as a key hotspot in the binding site of Snail protein. Meanwhile, the leucine-178 (L178) side pocket (in yellow) and the serine-257 (S257) hydrophobic pocket (in blue) are also important for the potential binding (Fig. 1, A and B, and fig. S1A). We then performed an established fragment-based virtual screening of the DrugBank database to seek the novel scaffolds (fig. S1B). We retrieved the fragment-like small molecules from the in-house chemical library and docked them in the Snail crystal structure [Protein Data Bank (PDB) ID: 3W5K] (32) using Glide docking algorithms. Small molecules that were able to form binding interactions (e.g., hydrogenic, hydrophobic, or noncovalent interactions) with R174 pocket were scored and ranked according to their Glide results. The docking poses of the top 200 ranked molecules were visually inspected. Fifty molecules representing 23 structural clusters with prior Glide scores were found to bind with R174 pocket (fig. S1C). Notably, we found that pyrrole-pyrimidine fragment (drugbank_431) may also occupy L178 side pocket and its amide group forms a hydrogenic binding interaction with the flexible R174 residue (Fig. 1B). However, the fragment is small and only occupies two binding pockets. As each pocket can describe the binding interaction between the pocket and its preferred moieties, we introduced a hydrophobic moiety to the pyrrole-pyrimidine fragment. Using a small library featured with hydrophobic fragments, we identified N-phenyl–substituted benzamide fragment as a suitable moiety that was predicted to occupy S257 hydrophobic pocket and maintain the compound's ability to form a hydrogenic binding interaction with R174 pocket (Fig. 1B). Using pyrrole-pyrimidine and N-phenyl–substituted benzamide fragments as the core scaffold, we designed and synthesized 17 compounds (fig. S1D). These compounds were docked into R174 pocket of Snail for the second round of filtration, and four compounds (i.e., CYD16 to CYD19) were found to form interaction with R174. As shown, the most potent compound CYD19 was predicted to anchor into Snail cavity by forming binding interactions with hotspot R174 pocket, L178 side pocket, and S257 hydrophobic pocket (Fig. 1, B and C). Next, we performed the biolayer interferometry (BLI) and microscale thermophoresis (MST) assays to measure the dissociation kinetics of CYD19. BLI analysis revealed that CYD19 had a submicromolar potency (K_d = 0.18 μM), while the inactive analog CYD18 was approximately 80-fold less potent toward Snail (K_d = 14.1 μM) (Fig. 1D). Similarly, MST assay showed that CYD19 was 55-fold more potent toward Snail than CYD18 (0.2 μM versus 11.1 μM in K_d) (fig. S1E). To further test whether R174 of Snail is important for its interaction with CYD19, we generated the Snail R174→A174 mutant (Snail-R174A mutant) and performed the BLI assay. We observed that the R174A

mutation caused steric conformation alteration due to dissimilarity of the side chain of residue, and thus, the compound CYD19 could not fit well with Snail-R174A mutant (Fig. 1C, compare right panel and left and middle panels). As expected, CYD19 showed a 16-fold lower binding affinity to Snail-R174A mutant (K_d = 3.0 μM) than wild-type Snail (Snail-WT), as assessed by a BLI assay (fig. S1F). Together, the results from the in silico and BLI assays suggest that R174 is essential for the high-affinity binding of Snail with CYD19. Because the C_2H_2-type zinc fingers (ZFs) are highly conserved across Snail family members, we used BLI assay to examine the dissociation kinetics of CYD19 toward Slug (alternatively termed Snail2), another member of the Snail family (6, 21, 33). As shown, CYD19 had a submicromolar potency (K_d = 0.6 μM), while the inactive analog CYD18 was approximately 145-fold less potent toward Slug protein (fig. S1G), suggesting that CYD19 also forms a binding interaction with Slug protein.

CYD19 functions as a potent CBP/p300-Snail interaction inhibitor

Next, we asked whether compound CYD19 could affect Snail expression in carcinoma cell cultures. Immunoblot analysis revealed that CYD19 dose-dependently decreased Snail protein levels in freshly isolated human BrCa primary cells, mouse and human BrCa cell lines, and colorectal cancer cell lines (Fig. 1E and fig. S2A). In addition, we observed that CYD19 reduced Snail protein levels in a time-dependent manner (fig. S2B). As expected, CYD18 did not affect Snail protein levels in the tested cell lines (fig. S2C). No significant changes in *Snail* mRNA levels were detected in CYD19-treated cells relative to control cells, suggesting that CYD19 regulated Snail expression at posttranslational level (fig. S2D). To directly test whether CYD19 could affect Snail protein stability, we cultured vehicle- or CYD19-treated mouse mammary tumor virus-polyoma middle tumor-antigen (MMTV-PyMT) cells in the presence of cycloheximide (CHX; 100 μg/ml) to block newly protein synthesis and examined Snail degradation. After treatment with CHX, Snail became unstable and degraded rapidly in CYD19-treated cells, while the protein was relatively stable in vehicle-treated cells, suggesting that CYD19 indeed reduces Snail protein stability (Fig. 1, F and G). Because CYD19 showed a significantly lower affinity with Snail-R174A mutant than Snail-WT, we compared the protein stability of Snail-R174A mutant versus Snail-WT following CYD19 treatment. Treatment of transfected human embryonic kidney (HEK) 293T cells with CYD19 diminished FLAG-tagged Snail-WT protein levels in a dose- and time-dependent manner (Fig. 1, H and I, top). However, treatment with CYD19 at up to 150 nM or for up to 48 hours failed to decrease Snail-R174A mutant protein levels (Fig. 1, H and I, bottom), confirming that R174 is a key amino acid for Snail's binding with CYD19. To test whether this CYD19 effect is mediated through a ubiquitination of Snail, we cotransfected HEK293T cells with FLAG-tagged Snail-WT (or Snail-R174A mutant) and hemagglutinin (HA)–ubiquitin and treated them with vehicle or CYD19 for 48 hours. MG132 (10 μM) was added to the cells 4 hours before cell harvesting, and the cell lysates were subjected to immunoprecipitation (IP) assay using an anti-FLAG antibody. Notably, we observed that CYD19 remarkably increased the ubiquitination levels of Snail-WT but failed to affect the ubiquitination of Snail-R174A mutant (Fig. 1J). The acetylation of Snail has been reported to stabilize Snail protein (18). We therefore asked whether CYD19 could affect Snail acetylation. We found that CYD19 remarkably decreased acetylation of Snail-WT but not
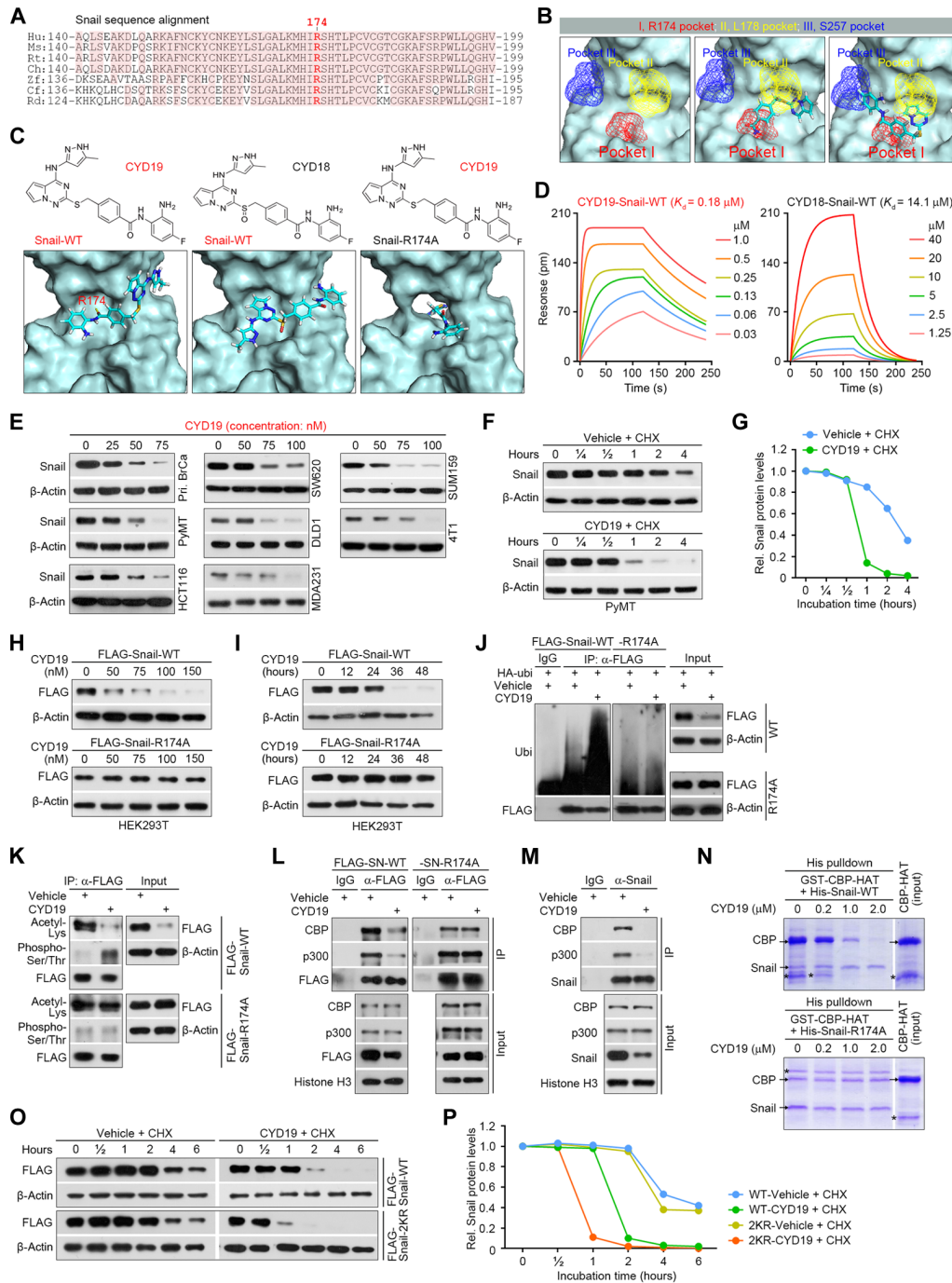
Fig. 1. CYD19 is a novel CBP/p300-Snail interaction inhibitor. (**A**) Diagram showing that R174 is evolutionarily conserved across species. Hu, human; Ms, mouse; Rt, rat; Ch, chimpanzee; Zf, zebra fish; Cf, clawed frog; Rd., rock dove. (**B**) Close-up view of three predicted binding pockets of Snail protein (left) and presumed interaction surface of pyrrole-pyrimidine fragment (middle) and hit compound (right) with Snail. (**C**) Molecular docking analysis. (**D**) BLI analysis to measure dissociation kinetics of compounds toward Snail recombinant proteins. (**E** and **F**) Immunoblot analysis of Snail expression in cancer cells treated with vehicle or CYD19 for 48 hours (E) or in MMTV-PyMT cells treated with vehicle or 50 nM CYD19 and then with cycloheximide (CHX; 100 μg/ml) for a total of 48 hours (F). MDA231, MDA-MB-231. (**G**) Densitometry of Snail protein in cells as described in (F). (**H** and **I**) Comparison of exogenous Snail-WT and Snail-R174A expressions in human embryonic kidney (HEK) 293T cells treated with vehicle or CYD19 for 48 hours (H) or in cells treated with vehicle or 50 nM CYD19 for different times (I). (**J**) Comparison of ubiquitinated Snail-WT and Snail-R174A proteins in HEK293T cells treated with vehicle or 50 nM CYD19 for 48 hours. MG132 (10 μM) was added 4 hours before harvesting. IgG, immunoglobulin G; IP, immunoprecipitation; HA-ubi, hemagglutinin-ubiquitin. (**K**) Comparison of acetylated and phosphorylated Snail-WT versus Snail-R174A proteins in HEK293T cells as described in (J). (**L** and **M**) Binding interaction of exogenous (L) or endogenous (M) Snail with endogenous CBP/p300 was monitored in cells that were treated with vehicle or 50 nM CYD19 for 48 hours. (**N**) His pulldown assay to assess CYD19's impact on association of CBP-HAT with Snail-WT or Snail-R174A. Arrows and asterisks mark specific and nonspecific bands, respectively. (**O**) Immunoblot analysis of exogenous Snail expression in HEK293T cells treated with vehicle or 50 nM CYD19 and then with CHX (100 μg/ml) for a total of 48 hours. (**P**) Densitometry of exogenous Snail protein in cells described in (O). All representative blots as shown are from three independent experiments.

Snail-R174A mutant proteins (Fig. 1M). GSK3β and PKD1 can phosphorylate Snail and promotes its ubiquitination and degradation (25–29). Snail acetylation can reduce its phosphorylation, which consequently results in increased protein stability (18). Here, we showed that treatment with CYD19 markedly increased phosphorylation levels of Snail-WT protein but had negligible effects on phosphorylation levels of Snail-R174A mutant protein (Fig. 1K). CBP/p300 has been reported to function as the primary HATs that may acetylate Snail at K146 and K187 (18). We therefore hypothesized that CYD19 binds to Snail protein, which consequently interrupts the interaction of Snail with CBP/p300 and results in impairment of Snail acetylation. To test this, we treated exogenous Snail-transfected HEK293T and HCT116 cells with vehicle or CYD19 and subjected the cell lysates to IP assays using anti-FLAG or anti-Snail antibodies, followed by immunoblot analysis using anti-CBP and anti-p300 antibodies (Fig. 1, L and M). We observed that the treatment of HEK293T and HCT116 cells with CYD19 did not affect total CBP/p300 expressions but markedly reduced Snail-bound CBP/p300 levels (Fig. 1, L and M). In notable contrast, CYD19 did not affect the binding of Snail-R174A mutant with CBP/p300 (Fig. 1L, right). To directly evaluate the ability of CYD19 to interfere the interaction between Snail and CBP, we expressed and purified glutathione S-transferase (GST)–CBP-HAT (containing HAT domain of CBP protein) and His-tagged Snail-WT and Snail-R174A (His-Snail-WT and His-Snail-R174A, respectively) mutant recombinant proteins in *Escherichia coli* bacteria and performed in vitro His pulldown experiments. We observed that CYD19 dose-dependently diminished the interaction of CBP-HAT with His-Snail-WT but not His-Snail-R174A mutant recombinant proteins, suggesting that CYD19 directly interferes the binding between CBP and Snail in a dose-dependent manner (Fig. 1N). To examine whether CBP/p300-mediated acetylation of Snail is actively involved in the regulation of Snail protein stability by CYD19, we generated the Snail-K146R/K187R (Snail-2KR) mutant and performed the CHX chase assay. We observed that the half-life of Snail-2KR mutant protein and Snail-WT protein was comparable in vehicle-treated cells (Fig. 1, O and P). However, Snail-2KR mutant protein degraded more rapidly than Snail-WT protein in CYD19-treated cells, suggesting that CBP/p300-mediated acetylation stabilizes Snail protein in the presence of CYD19 (Fig. 1, O and P). Because CYD19 can also form a binding interaction with Slug, we asked whether CYD19 has an impact on Slug protein expression. Unexpectedly, CYD19 did not affect Slug protein expression in a variety of cancer cell lines (fig. S2E). We demonstrated that Slug, unlike Snail, did not form a binding interaction with CBP/p300 (fig. S2F), suggesting that there should exist other potential regulator proteins (not CBP/p300) responsible for modulating Slug protein expression. These findings suggest that compound CYD19 does not interrupt Slug's interaction with its potential regulator proteins and thus loses the ability to affect Slug protein expression.

Importins (e.g., importin β) are reported to transport Snail protein into the nucleus by tightly interacting with several key amino acid residues within Snail's ZF domains, including K161, K170, K187, R191, W193 (tryptophan-193), Q196 (glutamine-196), R220, R224, and Q228 (32, 34, 35). Single mutation, double mutations, or multiple mutations in these residues efficiently (or completely) reduce the binding of Snail with importin β, thus severely impairing importin β–mediated nuclear import of Snail protein (32, 34). To assess whether R174 is required for Snail binding to importin β and whether CYD19 that specifically binds to R174 could affect Snail–importin β bind-

ing interaction, we performed serial His pulldown assays, followed by immunoblots using anti–importin β and anti-Snail antibodies (34). To this end, His-Snail-WT or His-Snail-R174A mutant recombinant proteins were purified, immobilized on Ni–nitrilotriacetic acid (NTA) agarose, and incubated, either in the absence or presence of various concentrations of CYD19, with a complete HEK293T cell lysates used as a source of importin β. As shown, both Snail-WT and Snail-R174A mutant proteins physically bound with importin β indistinguishably (fig. S2G), suggesting that R174 is not required for Snail binding to importin β. Furthermore, compound CYD19 at various concentrations failed to affect binding of Snail-WT with importin β (fig. S2H). In addition, we performed in-cell experiments to test whether mutation in R174 could affect Snail subcellular localization. To completely exclude the possibility that small molecules (smaller than 50 kDa) such as Snail protein can diffuse into the nucleus through nuclear pore complexes, we increased the sizes of green fluorescent protein (GFP)–Snail-WT and GFP-Snail-R174A proteins by fusing them to GST and transfected them into MCF7 BrCa cells (32, 34). Although GFP-GST was detected in the nucleus and cytoplasm, both GFP-Snail-WT and GFP-Snail-R174A mutant proteins were exclusively localized in the nucleus (fig. S2I), suggesting that R174 is not required for Snail binding to importin β and plays no role in importin β–mediated Snail nuclear import. Intracellular localization of Snail protein was also examined by cell fractionation. As shown, FLAG-tagged Snail-WT and Snail-R174A mutant proteins were both exclusively localized in the nucleus of vehicle- and CYD19-treated cells (fig. S2J). These findings suggest that compound CYD19 that forms binding interaction with R174 pocket of Snail protein does not affect Snail–importin β interaction and subsequent Snail subcellular localization. Together, our data support the mode of action by on-target effect of compound CYD19; that is, CYD19 specifically binding to hotspot R174 pocket of Snail protein disrupts the interaction of Snail with CBP/p300 and eventually triggers Snail protein degradation without affecting Snail–importin β interaction and subsequent Snail subcellular localization.

CYD19 blocks Snail-driven EMT, migration, and CSC expansion in aggressive cancer cells

Snail has been shown to induce EMT and promote migration and metastasis in various cancer types (5, 8). TGFβ signaling is known to activate EMT in epithelial-like cancer cells through transcriptionally inducing Snail (8). We therefore tested whether CYD19 could block TGFβ1/Snail-driven EMT phenotypes in cancer cells. To do this, we pretreated cells with vehicle or TGFβ1 (2 ng/ml) for 24 hours and further treated them with vehicle or various concentrations of CYD19 in combination with TGFβ1 (2 ng/ml) for another 48 hours. Notably, we found that CYD19 efficiently blocked TGFβ1/Snail-driven EMT phenotypes in freshly isolated human BrCa primary cells and various cancer cell lines, as evidenced by increased expression of epithelial marker (E-cadherin) and decreased expressions of mesenchymal markers such as vimentin, N-cadherin, and fibronectin (Fig. 2, A and B, and fig. S3A). Snail is also known to transcriptionally activate inflammatory cytokine genes such as tumor necrosis factor–α (TNFα), extension repair cross-complementation group 1 (ERCC1), C-C motif chemokine ligand 2 (CCL2), CCL5, and interleukin-8 (IL8) (18, 36, 37). We next examined the impact of CYD19 on TGFβ1/Snail-modulated cytokinome in cancer cells. We observed that CYD19 treatment completely abolished TGFβ1/Snail-mediated activation of the indicated inflammatory cytokine genes in human BrCa primary
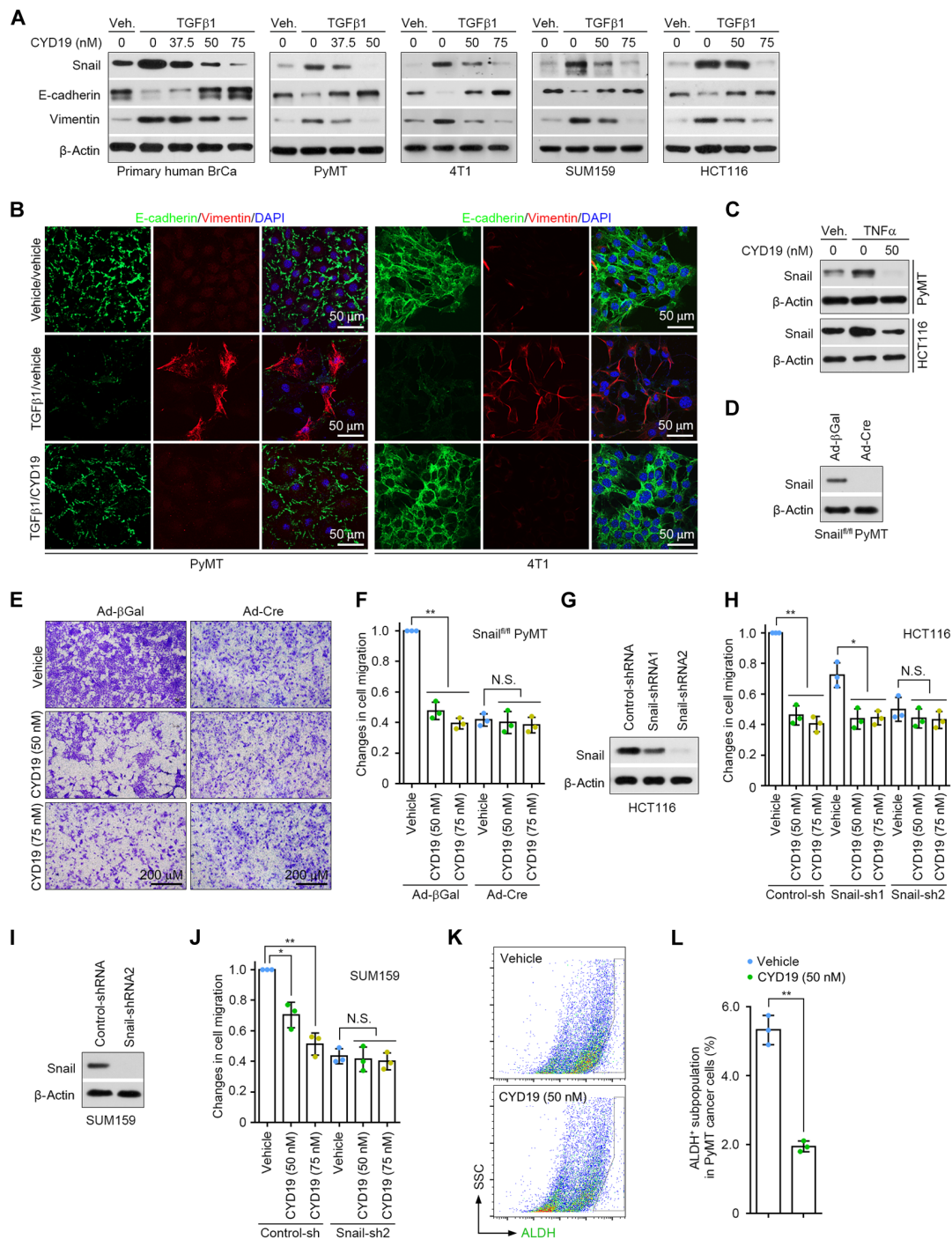
Fig. 2. CYD19 inhibits Snail-driven EMT, migration, and CSC expansion in aggressive cancer cells. (**A**) Immunoblot analysis of Snail, E-cadherin, and vimentin expressions in primary cancer cells and cancer cell lines that were treated with vehicle (Veh.) or TGFβ1 (2 ng/ml) for 24 hours and then with vehicle or CYD19 in the presence of TGFβ1 for another 48 hours. (**B**) Immunofluorescence staining of E-cadherin and vimentin in MMTV-PyMT (left) and 4T1 (right) cells as described in (A). Nuclei were counterstained with 4′,6-diamidino-2-phenylindole (DAPI) (blue). (**C**) Immunoblotting of Snail expression in MMTV-PyMT and HCT116 cells. Cells were treated with vehicle or CYD19 for 48 hours, and TNFα (10 ng/ml) was added 8 hours before cell harvesting. (**D**) Immunoblotting of Snail expression in Snail^{fl/fl} MMTV-PyMT cells that were infected with adeno-βGal or adeno-Cre vectors. (**E** and **F**) Equal numbers (2 × 10^{5} cells per well) of control and Snail-deleted MMTV-PyMT cells pretreated with vehicle or CYD19 for 48 hours were subjected to cell migration assays, and invaded cells were quantified (F). (**G** and **I**) Immunoblot analysis of Snail expression in HCT116 (G) and SUM159 (I) cells that were infected with lentiviral vectors expressing control–short hairpin–mediated RNA (shRNA) or two independent Snail-shRNAs. (**H** and **J**) Equal numbers (2 × 10^{5} cells per well) of HCT116 (H) and SUM159 (J) cells were subjected to cell migration assays, and invaded cells were quantified. (**K** and **L**) Representative histogram (K) and quantification (L) of ALDH[+] subpopulation in control and Snail-deleted MMTV-PyMT cells. All representative blots, images, and histograms as shown are from three independent experiments. All data are presented as means ± SD ($n = 3$ independent experiments). *$P < 0.05$ and **$P < 0.01$. N.S., not significant. Differences are tested using one-way analysis of variance (ANOVA) with Tukey's post hoc test (H and J) and unpaired two-tailed Student's t test (L).

cells and various cancer cell lines (fig. S3B), indicating the impact of CYD19 on tumor microenvironment remodeling during cancer progression. TNFα has been demonstrated to stabilize Snail protein by modulating nuclear factor κB signaling pathway (27). Thus, we evaluated the impact of CYD19 on TNFα-stimulated Snail expression. To do this, we treated cells with vehicle or CYD19 for 48 hours and added TNFα (10 ng/ml) to stimulate the cells 8 hours before cell harvesting. We found that CYD19 efficiently blocked TNFα-stimulated Snail protein expression (Fig. 2C). Together, these findings suggest the important role of CYD19 in suppressing the external stimulus–induced Snail expression. Given that Snail-induced EMT is closely related to migration and invasion of cancer cells, we examined the impact of CYD19 on cancer cell migration. To do this, equal numbers of vehicle- or CYD19-pretreated cells were cultured in serum-free medium supplemented with vehicle or CYD19 in the upper chambers of transwell inserts, while the lower chambers were filled with medium containing 10% serum. We found that CYD19 dose-dependently reduced migration of a variety of cancer cell lines (fig. S3C). To test whether CYD19 inhibited cell migration by specifically targeting Snail protein, we infected Snail^{fl/fl} MMTV-PyMT cancer cells, a cell line that was previously established in our laboratory (20), with adeno–β-galactosidase (βGal) or adeno-Cre to generate control or Snail-deleted cells, treated them with CYD19 (or vehicle), and subjected them to cell migration assay (Fig. 2, D to F). As expected, migration of Snail-deleted cells was markedly reduced compared to control cells, and CYD19 remarkably suppressed migration of control cells but largely failed to inhibit migration of Snail-deleted cells (Fig. 2, E and F). Moreover, we silenced Snail expression in HCT116 and SUM159 cells and then subjected the cells to migration analysis. As shown, cell migration was slightly reduced in HCT116 cells where Snail was moderately silenced but significantly reduced in cells where Snail was almost completely depleted; CYD19 efficiently reduced migration of control and Snail–moderately silenced HCT116 cells but did not affect migration of Snail–completely silenced cells (Fig. 2, G and H). A similar phenotype was also observed in SUM159 cells (Fig. 2, I and J). These results suggest that CYD19 inhibits cell migration by specifically targeting Snail protein. Recently, Snail has been reported to play a critical role in regulating aldehyde dehydrogenase–positive (ALDH[+]) CSC expansion in established MMTV-PyMT breast tumors (20, 38). Here, we observed substantially reduced numbers of ALDH[+] CSCs in CYD19-treated cells compared to vehicle-treated cells, suggesting that CYD19 blocked Snail-driven CSC expansion in MMTV-PyMT cells (Fig. 2, K and L).

CYD19 reverses Snail-dependent repression of wild-type p53
We previously showed that Snail interacts directly with wild-type, but not mutant, p53, thereby triggering its proteasome degradation in BrCa cells (20). Therefore, we asked whether CYD19 has an impact on expression of wild-type and mutant p53. Immunoblot analysis revealed that CYD19 dose-dependently increased wild-type p53 protein levels in various cell lines (Fig. 3A, left). In notable contrast, CYD19 did not affect mutant p53 protein expression in MDA-MB-231, SW620, and DLD1 cells (Fig. 3A, right). Immunofluorescence analysis revealed markedly decreased Snail expression in tandem with increased p53 expression in CYD19-treated MMTV-PyMT and HCT116 cells relative to control cells (Fig. 3B). Although CYD19 did not affect *TP53* expression, the compound did increase the mRNA and protein levels of p53 targets *p21* and *MDM2* in MMTV-PyMT and

HCT116 cells in a dose- and time-dependent manner (Fig. 3, C and D, and fig. S4, A and B). To test whether CYD19 could affect wild-type p53 protein stability, vehicle- or CYD19-treated MMTV-PyMT cells were cultured in the presence of CHX (100 μg/ml) to block newly protein synthesis, and p53 degradation was examined. After treatment with CHX, p53 protein in vehicle-treated cells was unstable and degraded rapidly starting from $^1/_2$ hours after CHX treatment, while p53 protein in CYD19-treated cells was more stable and started to degrade 2 hours after CHX treatment (Fig. 3, E and F), suggesting that CYD19 increases wild-type p53 protein stability. Consistently, we observed that CYD19 robustly decreased the ubiquitination of endogenous p53 in MMTV-PyMT cells (Fig. 3G). Notably, increase in p53 protein levels and activity are associated with increased levels of p53 acetylation (20, 39), and following Snail deletion, p53 acetylation levels increase (20). We found that CYD19 treatment of MMTV-PyMT cells exhibited increased levels of acetylated p53 (Fig. 3H), suggesting that CYD19 promotes p53 acetylation and thus stabilizes p53 protein by inhibiting Snail protein expression. We previously demonstrated that Snail binds to wild-type p53 and triggers p53 deacetylation by recruiting histone deacetylases (HDACs) to the complex (20). Here, we observed that CYD19 robustly diminished Snail-mediated binding interaction of wild-type p53 with HDAC1 (Fig. 3I), indicating that CYD19 disrupts the HDAC1 recruitment to wild-type p53 and thus increases p53 acetylation and protein levels. To directly test whether Snail is required for CYD19-mediated up-regulation on wild-type p53 expression, we compared expressions of p53 and its target protein p21 in control and Snail-deleted MMTV-PyMT cells in the presence of increasing concentrations of CYD19. Notably, we found that CYD19 robustly increased p53 and p21 expressions in control cells but largely failed to increase their expressions in Snail-deleted cells (Fig. 3J), suggesting that CYD19-mediated up-regulation on p53 pathway heavily depends on Snail expression. Snail silencing robustly increased expression of wild-type p53 protein in HCT116 cells but did not affect mutant p53 expression in DLD1 and SUM159 cells (fig. S4, C to E), confirming our previous observations (20).

CYD19 reduces proliferation and survival of cancer cells harboring wild-type p53
We previously identified Snail as a molecular bypass that suppresses the antiproliferative and proapoptotic effects exerted by wild-type p53 in BrCa (20). Because compound CYD19 increases protein expression of wild-type, but not mutant, p53, we asked whether the compound could affect proliferation and survival of cancer cells harboring wild-type or mutant p53. Notably, we observed that cells harboring wild-type p53 were significantly more sensitive to CYD19 treatment than cells expressing mutant p53, as assessed by the CCK-8 (cell counting kit-8) proliferation assay (Fig. 4A). Furthermore, CYD19 induced apoptosis in a dose-dependent manner in cells expressing wild-type p53 but essentially failed to induce apoptosis in cells with mutant p53 (Fig. 4B and fig. S5A). Consistently, treatment of wild-type p53-expressing MMTV-PyMT and HCT116 cells with compound CYD19 dose-dependently increased expressions of p53-inducible proapoptotic proteins Puma and Bax and triggered the release of cytochrome c (Cyt-c) from mitochondria, thus inducing the activation (cleavage) of caspase 9 and caspase 3, a dominant executor of cell apoptosis (Fig. 4C). CYD19 also increased Bax expression and induced caspase 3 activation in a time-dependent manner (fig. S5B). To determine whether Snail is required for CYD19-mediated
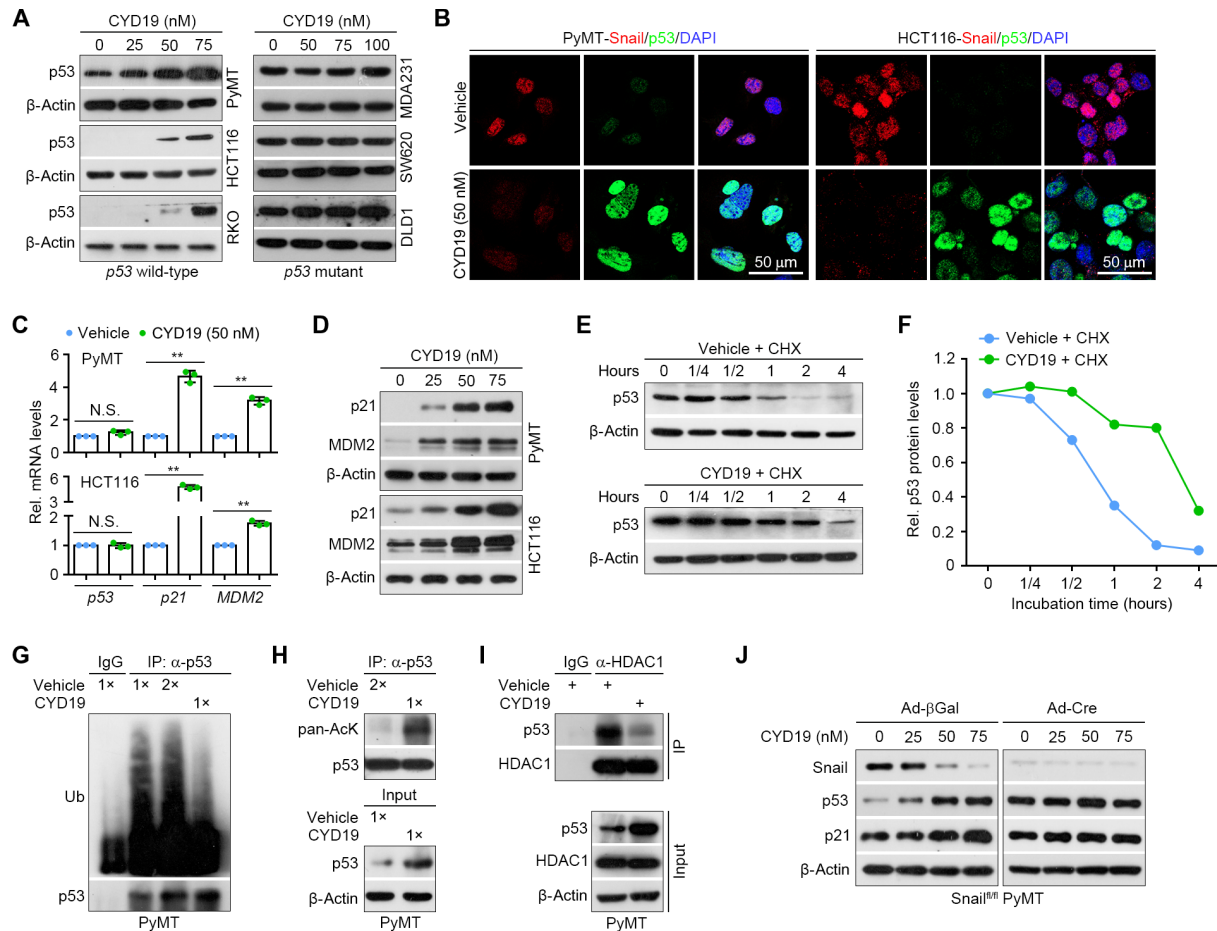
Fig. 3. CYD19 reverses Snail-dependent repression of wild-type p53. (**A**) Immunoblot analysis of p53 expression in wild-type (left) and mutant (right) p53-expressing cells that were treated with vehicle or CYD19 for 48 hours. (**B**) Immunofluorescence staining of Snail and p53 in MMTV-PyMT (left) and HCT116 (right) cells treated with vehicle or 50 nM CYD19 for 48 hours. (**C**) Reverse transcription quantitative polymerase chain reaction (qPCR) analysis of *p53*, *p21*, and *MDM2* expressions in MMTV-PyMT (top) and HCT116 (bottom) cells as described in (B). (**D**) Immunoblot analysis of p53, p21, and MDM2 expressions in MMTV-PyMT and HCT116 cells treated with vehicle or CYD19 for 48 hours. (**E**) Immunoblot analysis of p53 expression in MMTV-PyMT cells treated with vehicle or 50 nM CYD19 and then with CHX (100 μg/ml) for a total of 48 hours. (**F**) Densitometry of p53 protein in cells as described in (E). (**G**) Comparison of ubiquitinated p53 protein in vehicle- and CYD19-treated MMTV-PyMT cells. MG132 (10 μM) was added 4 hours before harvesting. Lysates from vehicle- and CYD19-treated cells loaded at ratios of 2:1 and 1:1 were subjected to IP assay using an anti-p53 antibody. (**H**) Comparison of acetylated p53 protein in vehicle- and CYD19-treated MMTV-PyMT cells as described in (G). (**I**) Comparison of binding interaction of p53 with HDAC1 in vehicle- and CYD19-treated MMTV-PyMT cells as described in (G). (**J**) Comparison of Snail, p53, and p21 expressions in control (left) and Snail-deleted (right) MMTV-PyMT cells that were treated with vehicle or CYD19 for 48 hours. All representative blots and images as shown are from three independent experiments. All data are presented as means ± SD (*n* = 3 independent experiments). **P < 0.01. Differences are tested using unpaired two-tailed Student's *t* test (C).

up-regulation on proapoptotic protein expressions, we compared their expressions in control and Snail-deleted MMTV-PyMT cells in the presence of increasing concentrations of CYD19. As shown, we observed that CYD19 dose-dependently increased Bax and activated caspase 3 expressions in control MMTV-PyMT cells, while the compound essentially failed to increase proapoptotic protein expressions in Snail-deleted cells (Fig. 4D). The CCK-8 cell proliferation assay further revealed that Snail-deleted MMTV-PyMT cells were substantially less sensitive to CYD19 treatment than control cells (Fig. 4E). To directly test whether Snail is required for CYD19-mediated inhibition on cell proliferation and survival, Snail expression was silenced in HCT116 cells, and cell proliferation and survival were assessed in control and Snail-silenced cells in the presence of vehicle or increasing concentrations of CYD19. As shown, we found that CYD19 dose-dependently induced apoptosis in con-

trol HCT116 cells but essentially failed to induce apoptosis in Snail-silenced cells (Fig. 4F and fig. S5C). Consistently, the CCK-8 cell proliferation assay revealed that Snail-silenced HCT116 cells were significantly less sensitive to CYD19 treatment than control cells (Fig. 4G). To further test whether p53 is required for CYD19-mediated inhibition on cell survival and proliferation, p53 expression were silenced in HCT116, and cell survival and proliferation were assessed in control and p53-silenced cells in the presence of vehicle or increasing concentrations of CYD19. As compared with control cells, p53-silenced HCT116 cells had significantly diminished responsiveness to CYD19 to inhibit cell survival and proliferation (Fig. 4, H and I, and fig. S5D). Notably, Snail silencing efficiently reduced proliferation of wild-type p53-expressing tumor cells but did not affect growth of mutant p53-expressing cells (fig. S5E), which confirms and extends our previous observations (*20*). Given that Snail-driven
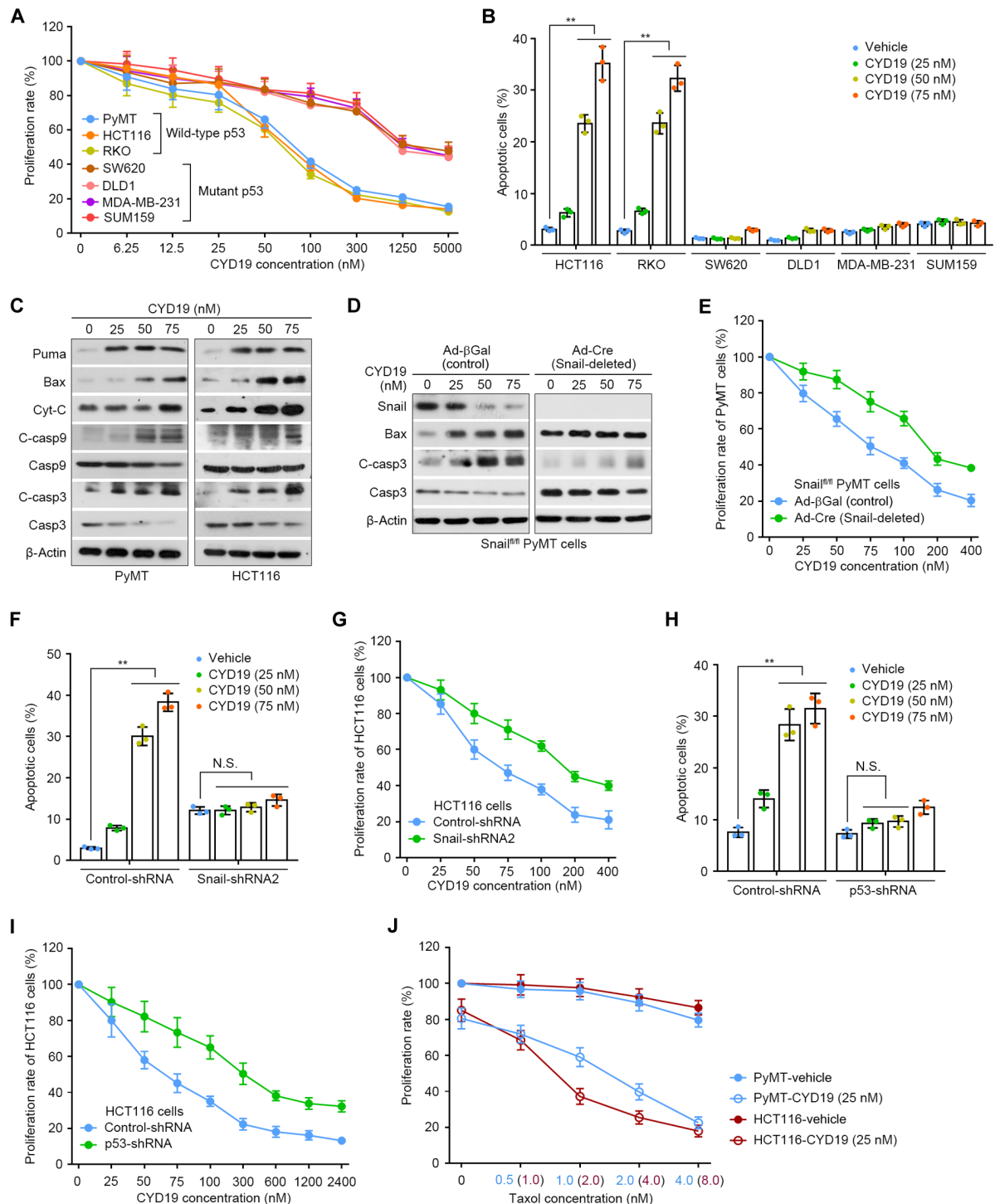
Fig. 4. CYD19 inhibits proliferation and survival of cancer cells expressing wild-type p53. (**A**) CCK-8 cell proliferation assay for wild-type and mutant p53-expressing cells treated with vehicle or CYD19 for 48 hours. (**B**) Quantification of apoptotic subpopulation in various cell lines treated with vehicle or CYD19 for 48 hours. (**C**) Immunoblot analysis of the indicated protein expressions in MMTV-PyMT (left) and HCT116 (right) cells as described in (B). C-casp9, cleaved caspase 9. (**D**) Immunoblot analysis of the indicated protein expressions in control and Snail-deleted MMTV-PyMT cells treated with vehicle or CYD19 for 48 hours. (**E**) CCK-8 analysis for control and Snail-deleted MMTV-PyMT cells treated with vehicle or CYD19 for 48 hours. (**F**) Quantification of apoptotic subpopulation in control and Snail-silenced HCT116 cells treated with vehicle or CYD19 for 48 hours. (**G**) CCK-8 analysis for control and Snail-silenced HCT116 cells treated with vehicle or CYD19 for 48 hours. (**H**) Quantification of apoptotic subpopulation in control and p53-silenced HCT116 cells treated with vehicle or CYD19 for 48 hours. (**I**) CCK-8 analysis for control and p53-silenced HCT116 cells treated with vehicle or CYD19 for 48 hours. (**J**) CCK-8 analysis for MMTV-PyMT and HCT116 cells that were treated with vehicle or taxol in combination with vehicle or 25 nM CYD19 for 48 hours. All representative blots as shown are from three independent experiments. All data are presented as means ± SD ($n = 3$ independent experiments). **$P < 0.01$. Differences are tested using one-way ANOVA with Tukey's post hoc test (B, F, and H).

EMT confers tumor resistance toward many chemotherapeutics (10, 15, 16), the impact of CYD19 on EMT-driven chemoresistance was therefore examined. We found that low-dose taxol (doses ranging from 0.5 to 4.0 nM in MMTV-PyMT cells and from 1.0 to 8.0 nM in HCT116 cells) or CYD19 (20 nM in both cell lines) had no impact on cell proliferation, while low-dose taxol in combination with CYD19 (25 nM) yielded a strong and superior antiproliferation activity in both cell lines (Fig. 4J), suggesting that CYD19 reverses EMT-driven chemoresistance and thus sensitizes cancer cells to low-dose chemotherapy. Together, our findings suggest that CYD19 reduces proliferation and survival of tumor cells in a *TP53* wild type–dependent fashion.

CYD19 inhibits Snail-driven tumor progression, pulmonary metastasis, and CSC expansion in MMTV-PyMT transgenic mice

Snail has been known to play an essential role in controlling tumor progression and metastasis as well as the expansion of TICs in MMTV-PyMT transgenic mice (20), a mouse model of BrCa that mirrors the multistep progression of human BrCa (40). Here, we asked whether CYD19 could affect Snail-driven progression and metastasis of spontaneous breast tumors in MMTV-PyMT transgenic mice. To do this, we treated 2-month-old female littermates that developed palpable breast tumors in a total volume of ~0.4 cm^3 with vehicle or CYD19 (30 mg/kg) for consecutive 25 days and examined the formation of primary and metastasized tumors. As shown, tumor volumes and weights were robustly reduced in CYD19-treated mice compared to vehicle-treated mice (Fig. 5, A and B). Notably, CYD19 did not affect body weights of tumor-bearing mice or induce detectable histological alterations in their vital organs such as the heart, liver, spleen, or kidneys, supporting the absence of toxicity in CYD19-treated mice (fig. S6, A and B). Furthermore, we observed that CYD19 substantially decreased the percentages of proliferative (Ki67-positive) and mitotic (phospho-histone H3–positive) cells but increased the percentages of apoptotic (cleaved caspase 3–positive) cells (Fig. 5, C and D, and fig. S6, C and D). As expected, tumors of CYD19-treated mice exhibited remarkably reduced Snail expression in tandem with increased wild-type p53 protein levels, as assessed by immunoblot and immunofluorescence analyses (Fig. 5E and fig. S6, E and F). Histological analysis revealed that vehicle-treated tumors progressed to poorly differentiated adenocarcinomas at the end of the treatment, while CYD19-treated tumors exhibited a more differentiated phenotype (Fig. 5F). Consistently, tumors of CYD19-treated mice showed an increase in E-cadherin expression in tandem with reduced vimentin expression, suggesting that CYD19 suppresses Snail-driven EMT in the in vivo setting (Fig. 5, G and H). We observed that CYD19 remarkably impaired ALDH$^+$ CSC expansion in primary tumors (Fig. 5, I and J), which is consistent with the in vitro observations (Fig. 2, M and N). Snail is known to promote recruitment of tumor-associated macrophages (TAMs), thus facilitating tumor progression (18). We observed that CYD19 reduced intratumoral infiltration of F4/80$^+$ TAMs and CD31$^+$ endothelial cells (Fig. 5, K and L). CYD19 also reduced metastatic potential of primary tumors, as evidenced by remarkably fewer and smaller metastatic nodules in the lungs of CYD19-treated mice relative to vehicle-treated mice (Fig. 5, M to O). Collectively, the findings suggest that CYD19 suppressed Snail-driven tumor progression, pulmonary metastasis, and CSC expansion in MMTV-PyMT transgenic mice that express wild-type p53.

CYD19 suppresses Snail-driven tumor growth, hepatic metastasis, and CSC expansion in colon cancer xenografts

Next, we asked whether CYD19 had a similar impact on colon cancer growth and hepatic metastasis using a HCT116 xenograft model in which 1×10^6 HCT116 cells in 50 μl of diluted Matrigel were injected subcutaneously into the dorsal flank of athymic BALB/c nude mice. We observed that CYD19 dose-dependently reduced the growth of HCT116 xenograft tumors (Fig. 6, A and B), without eliciting body weight loss or histological alterations in the vital organs such as the heart, liver, spleen, lung, and kidney (fig. S7, A and B). Furthermore, we found that CYD19 reduced the percentages of proliferative and mitotic cells while increasing the percentages of apoptotic cells in xenograft tumors (Fig. 6, C and D, and fig. S7, C and D). Notably, CYD19 suppressed Snail expression while increasing p53 expression in xenograft tumors, as assessed by immunoblot and immunohistochemical analyses (Fig. 6E and fig. S7, E to H). In addition, impaired EMT was detected in CYD19-treated xenograft tumors, as illustrated by increased E-cadherin expression in tandem with a reduction in vimentin expression (Fig. 6, F and G). We next examined the impact of CYD19 on ALDH$^+$ CSC expansion in HCT116 xenograft tumors. To do this, we sorted ALDH$^+$ and ALDH$^-$ cells from HCT116 xenograft tumors and performed in vitro tumorsphere assay. The results demonstrated that ALDH$^+$ but not ALDH$^-$ cells had the potential to form tumorspheres, confirming that ALDH can be used for identification of CSCs in HCT116 xenograft tumors (fig. S7I). Notably, we observed that CYD19 severely impaired ALDH$^+$ CSC expansion in HCT116 xenograft tumors (Fig. 6, H and I). To further examine whether the in vivo anticancer effect of CYD19 is Snail-dependent, we subcutaneously implanted 1×10^6 control or 2×10^6 Snail-silenced HCT116 cells into nude mice, treated mice with vehicle or CYD19 (30 mg/kg) for two consecutive weeks starting at 7 days after implantation, and monitored tumor growth. The volumes of xenograft tumors formed by 1×10^6 control or 2×10^6 Snail-silenced cells were comparable (Fig. 6J). Notably, CYD19 suppressed tumor growth of control cells but largely failed to affect tumor growth of Snail-silenced cells (Fig. 6J), suggesting that CYD19 suppresses tumor growth by specifically targeting Snail protein. Furthermore, immunoblot analysis of xenograft tumor lysates revealed that Snail expression was efficiently silenced in Snail–short hairpin–mediated RNA 2 (shRNA2)–expressing cells where p53 protein was robustly increased (Fig. 6K, compare lane 3 versus lane 1). As expected, CYD19 decreased Snail expression while increasing p53 protein in control cells (Fig. 6K, compare lane 2 versus lane 1), and the compound lost its ability to increase p53 expression in Snail-silenced cells (Fig. 6K, compare lane 4 versus lane 3). In addition, equal numbers (1×10^6) of control or Snail-silenced HCT116 cells were implanted into nude mice; the mice were treated with vehicle or CYD19, and tumor growth was monitored. As shown in fig. S7J, CYD19 suppressed tumor growth of control cells by 60.3% at the end point of treatment (compare curve 2 versus curve 1), and Snail silencing itself reduced tumor growth by 64.8% (compare curve 3 versus curve 1). While CYD19 remarkably reduced control tumor growth by 60.3%, the compound inhibited tumor growth of Snail-silenced cells by 4% (compare curve 4 versus curve 3), further confirming that CYD19 suppresses tumor growth by specifically targeting Snail protein. Next, we assessed the impact of CYD19 on tumor metastasis using a hepatic metastasis model in which 1×10^6 GFP-labeled HCT116 cells were intrasplenically injected to nude mice. The results demonstrated that CYD19 treatment for three consecutive
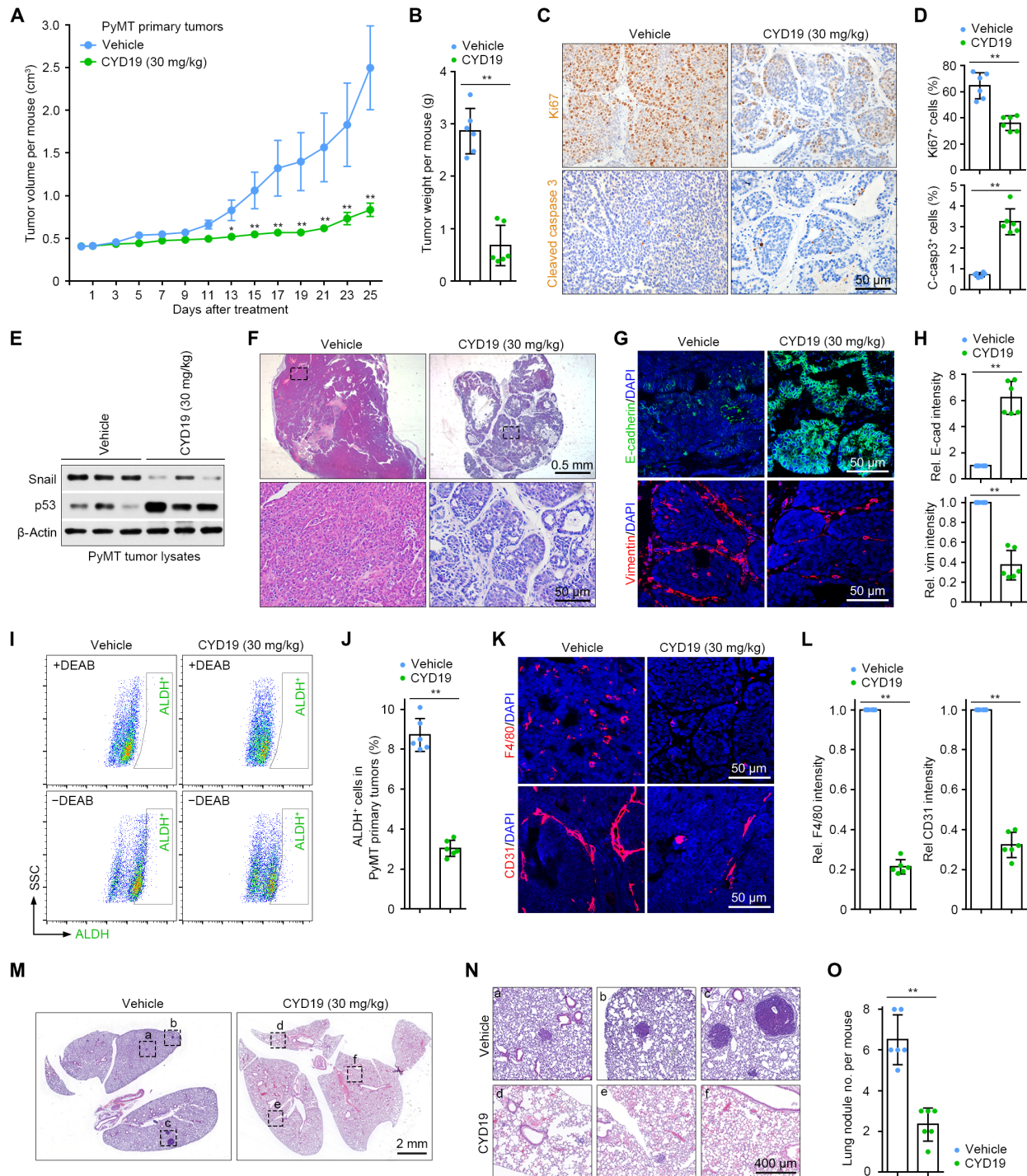
Fig. 5. CYD19 impairs Snail-driven tumor progression and pulmonary metastasis in MMTV-PyMT mice. (**A** and **B**) Primary tumor volumes (A) and weights (B) were measured in MMTV-PyMT mice that were intraperitoneally treated with vehicle or CYD19 (30 mg/kg) for 25 consecutive days (*n* = 6 mice, each). (**C**) Immunohistochemical staining of Ki67 (top) and cleaved caspase 3 (bottom) in primary tumors of vehicle- and CYD19-treated mice (*n* = 6 mice, each). (**D**) Quantification of Ki67-positive (Ki67^{+}; top) and cleaved caspase 3–positive (C-casp3[+]; bottom) cells in tumors as described in (C). (**E**) Immunoblot analysis of Snail and p53 expressions in tumor lysates of vehicle- and CYD19-treated mice (*n* = 3 pools from six mice, each). (**F**) Hematoxylin and eosin (H&E) staining for primary tumors as described in (C) (*n* = 6 mice, each). Magnified areas of boxed sections are shown in the bottom panels. (**G**) Immunofluorescence staining of E-cadherin and vimentin in primary tumors as described in (C) (*n* = 6 mice, each). (**H**) Quantification of staining intensity in primary tumors as described in (G). (**I** and **J**) Representative histogram (I) and quantification (J) of ALDH[+] subpopulation in primary tumors as described in (C) (*n* = 6 mice, each). DEAB, diethylaminobenzaldehyde. (**K**) Immunofluorescence staining of F4/80 and CD31 in primary tumors as described in (C) (*n* = 6 mice, each). (**L**) Quantification of staining intensity in primary tumors as described in (K). (**M**) H&E staining for vehicle- and CYD19-treated lungs (*n* = 6 mice, each). (**N**) Magnified areas of boxed sections in (M) are shown. (**O**) Quantification of nodules in vehicle- and CYD19-treated lungs as described in (M). All data are presented as means ± SD (*n* = 6 independent experiments). *P < 0.05 and **P < 0.01. Differences are tested using Mann-Whitney *U* test.

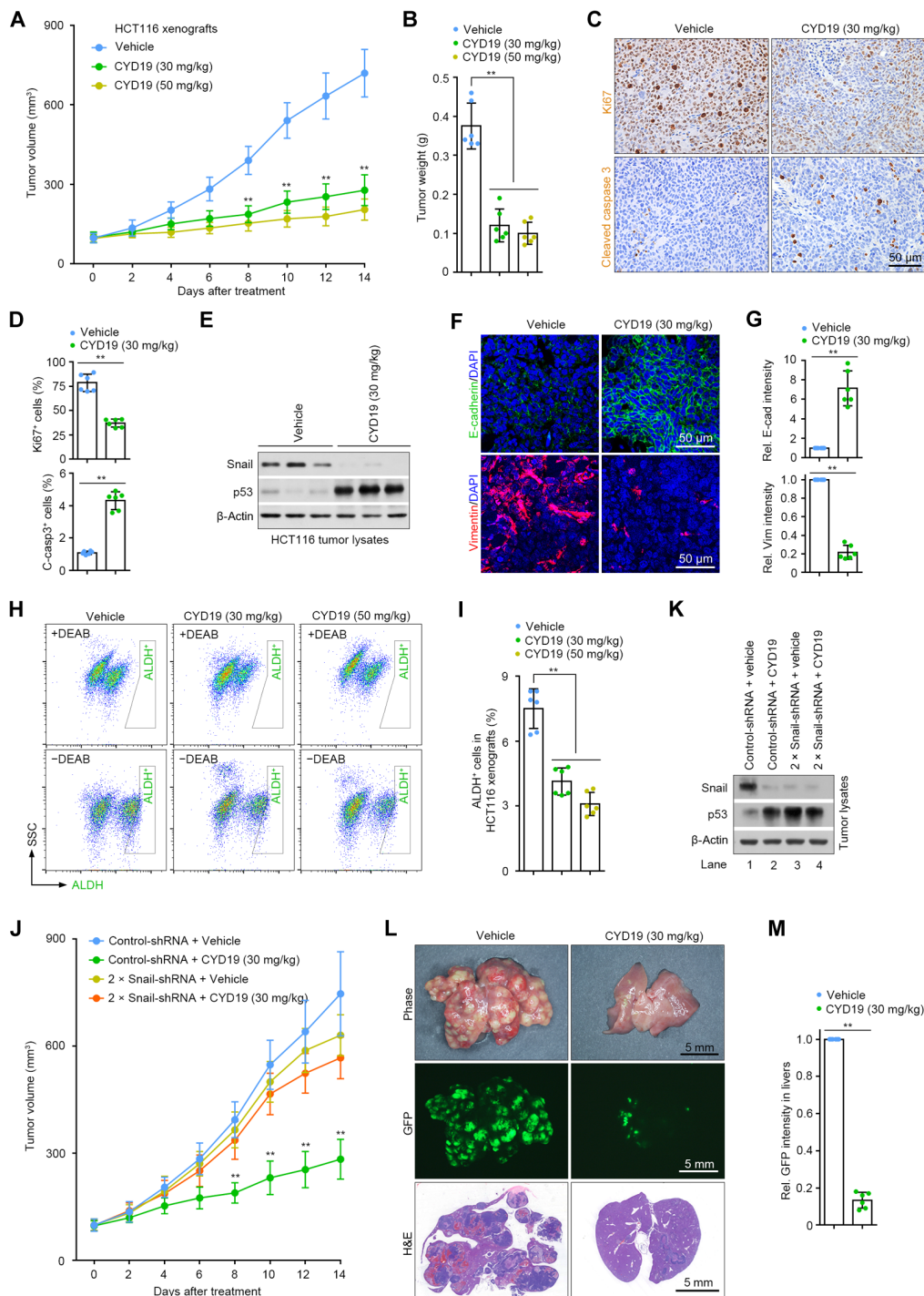**Fig. 6. CYD19 suppresses Snail-driven tumor growth and hepatic metastasis in colon cancer xenografts.** (**A** and **B**) HCT116 xenograft tumor volumes (A) and weights (B) were measured in athymic nude mice that were intraperitoneally treated with vehicle or CYD19 for two consecutive weeks ($n = 6$ mice, each). (**C**) Immunohistochemical staining of Ki67 (top) and cleaved caspase 3 (bottom) in xenograft tumors of vehicle- and CYD19-treated mice ($n = 6$ mice, each). (**D**) Quantification of Ki67$^+$ (top) and C-casp3$^+$ (bottom) cells in tumors as described in (C). (**E**) Immunoblot analysis of Snail and p53 expressions in tumor lysates of vehicle- and CYD19-treated mice ($n = 3$ pools from six mice, each). (**F**) Immunofluorescence staining of E-cadherin and vimentin in xenograft tumors of vehicle- and CYD19-treated mice ($n = 6$ mice, each). (**G**) Quantification of staining intensity in xenograft tumors as described in (F). (**H** and **I**) Representative histogram (H) and quantification (I) of ALDH$^+$ subpopulation in xenograft tumors as described in (C) ($n = 6$ mice, each). (**J**) Growth of HCT116 xenograft tumors derived from 1×10^6 control cells or 2×10^6 Snail-silenced cells was monitored in nude mice treated with vehicle or CYD19 for two consecutive weeks ($n = 6$ mice, each). (**K**) Immunoblot analysis of Snail and p53 expressions in lysates of xenograft tumors as described in (J). (**L**) Representative phase contrast (top), GFP fluorescence (middle), and H&E (bottom) images of vehicle- and CYD19-treated livers ($n = 6$ mice, each). Mice were treated with vehicle or CYD19 for three consecutive weeks starting from the third day after surgery. (**M**) Quantification of fluorescence intensity in livers as described in (L). All data are presented as means ± SD ($n = 6$ independent experiments). **$P < 0.01$. Differences are tested using Mann-Whitney U test.

weeks robustly reduced tumor metastasis and nodule formation in the livers (Fig. 6, L and M). Together, these findings suggest that CYD19 reduces Snail-driven tumor growth, hepatic metastasis, and CSC expansion in colon cancer xenografts expressing wild-type p53.

DISCUSSION

The ZF transcription factor Snail is aberrantly activated in a variety of malignant tumor types (*20–23*) and plays an essential role in EMT, metastasis, stem cell–like properties, cancer metabolism, micro-environment modulation, immune evasion, cancer recurrence, and therapeutic resistance (*9, 10, 13–18, 41, 42*). Snail is also known to promote cancer cell survival by enhancing resistance to apoptosis under the genotoxic stress condition (*19*). We recently identified Snail as a molecular bypass that suppresses the antiproliferative and proapoptotic effect in BrCa (*20*). Given the important role of Snail in driving cancer progression, we propose that targeting Snail would be an attractive anticancer therapeutic approach. However, to our knowledge, the development of small molecules to inhibit Snail's functions is unsuccessful, as there is no clear "ligand-binding domain" for targeting Snail (*43*). In the current study, we have identified the evolutionarily conserved R174 pocket as a key hotspot in the binding site of Snail. Using fragment-based virtual screening analysis in combination with Glide docking algorithms, we have screened 50 small molecules that represent 23 structural clusters. Using the pyrrole-pyrimidine fragment and *N*-phenyl–substituted benzamide fragment as the core scaffold, we then designed 17 small-molecule compounds. Using BLI and MST analyses, the compound CYD19 that is predicted to form both hydrogenic and hydrophobic binding interactions with R174 pocket has been eventually identified as a lead compound showing the highest binding affinity with recombinant Snail protein among these compounds. BLI analysis reveals that Snail-R174A mutant protein is 16-fold less potent toward CYD19 than Snail-WT protein. Serial biochemical analyses further show that Snail-WT protein can be efficiently captured by CYD19 and is consequently degraded through the ubiquitin-proteasome pathway, while Snail-R174A mutant protein is essentially resistant to degradation following CYD19 treatment because of its inefficient interaction with CYD19. On the basis of these observations, we conclude that the evolutionarily conserved R174 pocket instead of the ligand-binding domain within Snail protein is critical for its interaction with the compound CYD19.

CBP/p300 HATs have been shown to bind to acetylate and stabilize Snail by repressing its polyubiquitination and subsequent proteasome degradation (*18*). Note that CYD19 binding to Snail has no impact on the interaction of Snail with importin β1, thus failing to affect importin β1–mediated nuclear import of Snail protein. On the basis of Snail–importin β1 cocrystal structure (*32*), we propose that CYD19 binds to the outer surface of Snail–importin β1 complex and thus impairs the surface contact–mediated Snail-CBP/p300 interaction. Following treatment of cancer cells with CYD19, Snail acetylation level is reduced while its levels of phosphorylation and ubiquitination are increased, thereby promoting proteasome degradation of Snail. Two phosphorylation-dependent E3 ligases β-TRCP and FBXO11 and one phosphorylation-independent E3 ligase FBXL14 have been identified that mediate Snail degradation (*25–31*). Although we observed that CYD19-treated cells increased the phosphorylation levels of Snail, we could not exclude the possibility that FBXL14 is also responsible for Snail degradation. Snail is abundantly expressed in

specific cell lineages during embryonic development, becomes essentially undetectable in normal adult tissues, and is reactivated in cancerous tissues, revealing the spatial and temporal expression pattern of Snail in normal and neoplastic states (*7, 20–23, 44, 45*). Notably, we have observed that CYD19 potently suppresses Snail-driven cancer growth and metastasis without eliciting obvious side toxicity in tumor-bearing mice. This can be attributed to the high selectivity of the compound for targeting Snail protein and the spatial expression pattern of Snail in cancerous tissues versus normal tissues (*7, 20–23, 44, 45*). Since CYD19 specifically interrupts the binding interaction of CBP/p300 with Snail without affecting its enzymic activity, we expect that CYD19 may have a significantly lower toxicity than the enzyme inhibitors of CBP/p300 or deubiquitinases 3, two enzymes that may affect expression of many downstream proteins including Snail protein (*18, 43*). Notably, Slug, unlike Snail, cannot form a binding interaction with CBP/p300, and there should exist other potential regulator proteins responsible for modulating Slug protein expression. We therefore propose that compound CYD19 does not interrupt Slug's interaction with its regulator proteins and thus loses the ability to affect Slug protein expression. Future work is needed to identify the regulator proteins that are responsible for modulating Slug protein expression.

The tumor suppressor p53 protein is stabilized and activated in response to cellular stress, thereby triggering growth arrest and apoptosis in cancer cells. *TP53* is a frequent mutational target in human cancers (~50%), and mutant p53 loses the function of wild-type p53 but functions as an oncoprotein instead (*46*). The EMT-associated transcription factors, including Slug, Zinc Finger E-Box Binding Homeobox 1 (ZEB1), and Twist, have been reported to indirectly or directly affect p53 function, but the outcome of these interactions has varied (*19, 47, 48*). Using a MMTV-PyMT BrCa mouse model, we recently find that Snail deletion stabilizes wild-type, but not mutant, p53 and identify Snail as a molecular bypass that suppresses the antiproliferative and proapoptotic effects executed by wild-type p53 (*20*). Here, we further present in vitro data demonstrating that silencing Snail robustly reduces growth of wild-type p53–expressing tumor cells but does not affect growth of tumor cells expressing mutant p53. Snail deficiency in embryonic endothelial cells epigenetically enhances Delta Like Canonical Notch Ligand 4 (DLL4)/ Notch signaling but does not affect wild-type p53 protein expression, which consequently represses embryonic vascular remodeling without affecting proliferation or survival of endothelial cells (*44*). On the basis of these observations, we propose that Snail functions as a key regulator in tumor progression and embryonic vascular development through two distinct mechanisms.

In the present study, we found that compound CYD19 specifically binds to hotspot R174 pocket of Snail protein and thus disrupts the binding interaction of Snail with CBP/p300, which eventually triggers Snail protein degradation through the ubiquitin-proteasome pathway. CYD19 restores Snail-dependent repression of wild-type p53 and thus reduces tumor cell growth and survival. CYD19 also reverses Snail-driven EMT and impairs EMT-associated tumor invasion and metastasis. Given that aberrantly activated Snail is associated with poor prognosis and that more than 50% of patients with cancer express wild-type p53, pharmacologically targeting Snail by CYD19 may exert good therapeutic benefits in patients with cancer especially harboring wild-type p53. Moreover, pharmacologically targeting Snail by CYD19 may also diminish EMT-associated therapeutic resistance and thus sensitizes tumors to low-dose chemotherapy,

supporting the rationale for the combination of CYD19 with non-toxic low-dose chemotherapeutics for cancer treatment in the clinic.

MATERIALS AND METHODS

Collection of mouse and human tumor samples

Mice were housed under standard specific pathogen–free conditions, and all animal experiments were performed in accordance with protocols approved by the Animal Ethics Committee of China Pharmaceutical University. MMTV-PyMT transgenic mice on FVB background were purchased from the Jackson laboratory (#002374), and the colony was maintained in our laboratory. Male athymic BALB/c nu/nu nude mice were obtained from Qinglongshan Animal Facility (Nanjing, China). The maximal tumor sizes permitted under the approved protocols are 3 cm (length) by 3 cm (width). The clinical study was approved by the Ethics Committee of the First Affiliated Hospital of Nanjing Medical University, and written informed consents were obtained from each participant before procedure.

Molecular docking and compound designing strategy

The crystal structure of Snail has been reported (32), thus offering an opportunity for structure-based drug design. FTMap, an online computational solvent mapping software (http://ftmap.bu.edu/login.php), was applied to predict the binding hotspots of a protein by using a set of 16 small organic molecules (that is, probes) that vary in size, shape, and polarity. The probes were applied to find favorable positions using an empirical energy function and the CHARMM potential with a continuum electrostatics term. The regions that bind several small organic probe clusters are defined as the predicted hotspots. The residues with the highest number of interactions are defined as the main hotspots. The druggable binding cleft of Snail (PDB ID: 3W5K) (32) mainly consists of three main subpockets: R174 pocket, L178 side pocket, and S257 hydrophobic pocket. For each pocket, a set of chemically related fragments were identified. On the basis of the DrugBank database for virtual screening, an in-house chemical library containing fragment-like molecules was prepared to explore the potential small molecules that form a high-affinity binding interaction with Snail protein. The DrugBank database (http://www.drugbank.ca), which consists of 7736 drug items (including 1584 Food and Drug Administration–approved small-molecule drugs), was applied for drug screening. For virtual screening, the simulations were applied through the software "Schrödinger 2016." Preparation of the crystal structures of Snail (32) was carried out using the Protein Preparation Wizard module. Proper preparation of the ligands was accomplished by the LigPrep module. All other parameters were set to the default values. The cavity that surrounds within 15 Å of the R174 pocket was defined as the binding site. Top-ranking 200 molecules were picked up for visual observation based on docking scores of Glide_SP module. These molecules were then filtered on the basis of the predefined interaction to the Snail crystal structure. The pyrrole-pyrimidine (DrugBank_431) fragment could form close atomic contacts with residues in both R174 binding pocket and L178 binding pocket. The molecules were further optimized to improve the compounds' shape complementarity to the third S257 hydrophobic binding pocket. A small-molecule library featured by hydrophobic fragments was applied to screen the appropriate hit compounds. Both pyrrole-pyrimidine and N-phenyl–substituted benzamide fragments were predicted to match Snail protein: (i) engaging in H bond–acceptor interactions with the backbone residue of R174 (hinge binding region), (ii) occupying S257 hydrophobic pocket, and (iii) positioning an aromatic group to make edge-to-face interaction with L178 side pocket. Last, 17 candidate compounds were selected and synthesized for further docking and experimental validation.

Compound synthesis

Details of the organic synthesis and chemical characterization of the compounds are available upon reasonable request. Compounds used in assays were dissolved in 100% dimethyl sulfoxide and kept as 50 mM stock solutions for in vitro studies.

Cell isolation and culture

All cell lines used in the study were purchased from the American Type Culture Collection. Cells were tested for mycoplasma contamination every 1 month, and only mycoplasma-negative cells were used. Wild-type and Snail$^{fl/fl}$ MMTV-PyMT cancer cells were generated and maintained in our laboratory as described previously (20). MMTV-PyMT cancer cells were cultured in Dulbecco's modified Eagle's medium (DMEM)/F12 medium supplemented with 5% heat-inactivated fetal bovine serum (FBS) (Thermo Fisher Scientific, #10099-147), EGF (10 ng/ml; PeproTech, #315-09), hydrocortisone (500 ng/ml; Sigma-Aldrich, #H0888), insulin (5 mg/ml; #I9278), cholera toxin (20 ng/ml; #C8052), and 1% penicillin-streptomycin (Thermo Fisher Scientific, #15140122). HEK293T, HCT116, RKO, 4T1, DLD1, SW620, SUM159, and MDA-MB-231 cells were grown in DMEM supplemented with 10% FBS and 1% penicillin-streptomycin. For isolation of human BrCa primary cells, freshly isolated breast tumors were rinsed extensively three times in cold phosphate-buffered saline (PBS) supplemented with 1% penicillin-streptomycin and chopped into small fragments (~1 mm^3). Tissue fragments were digested into single-cell suspension by incubation in DMEM containing 10% FBS, 1% penicillin-streptomycin, collagenase type 1 (1 mg/ml; Sigma-Aldrich, #C0130), and hyaluronidase (125 U/ml; STEMCELL Technologies, #07919) for 12 to 18 hours at 37°C with slow agitation. After incubating for 5 min at room temperature without agitation, the stromal cell–enriched supernatant was discarded, and the epithelial cell–rich pellets were filtered with a 40-µm nylon mesh to remove cell clumps. Tumor epithelial cells were washed three times, resuspended, and cultured in DMEM/F12 medium containing 5% heat-inactivated FBS, EGF (10 ng/ml), hydrocortisone (500 ng/ml), insulin (5 mg/ml), cholera toxin (20 ng/ml), and 1% penicillin-streptomycin.

BLI assay

The binding of various concentrations of CYD19 to Snail-R174A mutant proteins was determined using BLI assays with an Octet RED96 instrument (ForteBio). Briefly, recombinant Snail-R174A mutant proteins were dissolved in PBS. For biotin labeling, EZ-Link NHS-Biotin was incubated for 60 min with proteins at room temperature (1:3 molar ratio of protein to biotin). Desalination was used to remove the excess of biotin. The biotinylated protein was immobilized onto Super Streptavidin (SSA) biosensors for further measurement. A duplicate set of SSA sensors incubated in the buffer without protein were used as negative binding control. The assay was determined in black 96-well plates at different concentrations of CYD19 and PBS as a nonspecific interaction control. The binding event was recorded according to the shift in the interference pattern of the light. Data were then analyzed in ForteBio Data Analysis to calculate the association and dissociation rates using 1:1 binding model, and K_d was represented by the ratio K_{off}/K_{on}.

MST assay

A Monolith NT.115 purchased from NanoTemper Technologies was used for MST assays. The concentration of GFP-tagged Snail recombinant protein was diluted according to the manufacturer's instructions. The selected compounds at different concentrations were incubated with GFP-tagged Snail protein for 5 min at room temperature in assay buffer containing 0.05% Tween 20. Thermophoresis was then determined at 25°C with 20 to 50% excitation power and 40 to 60% MST power.

Protein expression and purification

Recombinant His-tagged Snail protein was purified from *E. coli* (BL21) by Ni-NTA affinity chromatography. Cells were lysed in lysis buffer [containing 10 mM MgCl$_2$, 150 mM NaCl, 20 mM tris-HCl (pH 8.0), and 10 mM imidazole] and eluted stepwise using 50, 300, and 500 mM imidazole in wash buffer. The eluted protein was further purified by size exclusion chromatography using a Superdex 75 (Millipore) equilibrated with 20 mM Hepes (pH 7.0), 50 mM NaCl, and 2 mM tris(2-carboxyethyl)phosphine (TCEP). Recombinant GST-tagged CBP-HAT protein was purified from *E. coli* (BL21) by affinity glutathione-agarose chromatography. Cells were lysed in STE buffer [containing 10 mM tris-HCl buffer, 100 mM NaCl, 1 mM EDTA, 0.01% Triton X-100, and 1 mM dithiothreitol (pH 7.5)] and eluted stepwise using elute buffer [200 mM tris-HCl and 30 mM L-glutathione reduced (pH 8.0)].

Flow cytometric analysis

For apoptosis analysis, cancer cells were treated with vehicle or various concentrations of CYD19 for 48 hours, and the percentage of apoptotic cells was determined by the fluorescein isothiocyanate annexin V apoptosis detection kit I (BD Biosciences, #556547) according to the manufacturer's instructions. The cell apoptosis was analyzed with FlowJo software. For ALDH activity analysis, tumors were chopped into small fragments (around 1 mm^3), digested into single-cell suspension by incubation in digestion buffer [0.1% collagenase type 2 (Sigma-Aldrich, #C6885) and deoxyribonuclease I (3 U/ml; Sigma-Aldrich, #D5025)] for 30 min at 37°C, and then filtered with a 40-μm nylon mesh to remove cell clumps. The single-cell suspensions or cancer cell lines were subjected to serial incubations with an antibody cocktail containing CD31, CD45, and Ter119 (STEMCELL Technologies, #19757C.1); a secondary biotin-labeled antibody cocktail (STEMCELL Technologies, #19153); and magnetic beads (15 min each) on ice (STEMCELL Technologies, #19150). The unbound cells were collected, and the bound cells were discarded. Cells were washed extensively and subjected to ALDH activity assay using a kit from STEMCELL Technologies according to the manufacturer's instructions. For each sample, half of the cells were treated with diethylaminobenzaldehyde (DEAB), and the other half were incubated with an activated ALDEFLUOR reagent. Gating was established using fixable viability dye exclusion for viability, and DEAB-treated cells were used to define negative gates. Flow cytometry data were collected with a MACSQuant flow cytometer (BD Biosciences), and analysis was conducted using FlowJo software.

Cell migration assay

Cells were treated with vehicle or various concentrations of CYD19 for 48 hours, and equal numbers (2×10^5 cells per well) of the cells were seeded in FBS-free DMEM culture medium in the presence of vehicle or various concentrations of CYD19 in the upper chambers of transwell inserts with an 8-μm pore size (BD Biosciences, #354480). The lower chambers were filled with 1 ml of complete medium supplemented with 10% FBS. Cells were allowed to invade the bottom chamber for 12 or 18 hours. Noninvading cells in the upper surface were removed, and invaded cells on the lower surface were fixed with 90% methanol and stained with 0.1% crystal violet for 5 min. The stained cells were photographed and quantified.

Cell proliferation assay

Cell proliferation was measured by a CCK-8 kit (Yeasen, #40203ES60) according to the manufacturer's instructions. Briefly, cells were seeded in 96-well plates at 4×10^3 cells per well in culture medium supplemented with 10% FBS. Cells were allowed to adhere for 12 hours and then treated with vehicle or various concentrations of CYD19 for another 48 hours. Cell proliferation was measured, and absorbance intensity was determined with a Molecular Devices microplate reader at 450 nm.

Tumor xenograft and liver metastasis models

Single-cell suspensions of 1×10^6 HCT116 cells in 50 μl of diluted Matrigel (1:1; BD Biosciences, #356234) were injected subcutaneously into the dorsal flank of male nude mice at 6 to 8 weeks of age. Mice were randomized into three groups until their tumors reached a size of approximately 100 mm^3. Mice were then treated with vehicle [formulated in ethanol/cremophor/water at 10:10:80 (v/v/v)], CYD19 (30 mg/kg), or CYD19 (50 mg/kg) via intraperitoneal injection for two consecutive weeks. Tumor volumes were measured every 1 day using the formula $\pi \times \text{length} \times \text{width}^2/6$. At the end point of treatment, mice were euthanized, and tumors and key organs were dissected, photographed, and weighed. Tissues were either fixed in 4% paraformaldehyde (PFA) for immunohistochemical and histological analyses or snap-frozen in liquid N$_2$ and stored at −80°C for immunoblot analysis. In some experiments, 1×10^6 control-shRNA–expressing cells and 2×10^6 (or 1×10^6) Snail-shRNA2–expressing cells were used to form tumor xenografts in comparable sizes. For liver metastasis assay, a left subcostal surgical incision was created, and 1×10^6 GFP-labeled HCT116 cells were intrasplenically injected into the spleen of male nude mice (6 to 8 weeks of age). Mice were then treated intraperitoneally with vehicle or CYD19 (30 mg/kg) for three consecutive weeks starting from the third day after surgery, and livers were then harvested for analysis.

MMTV-PyMT mouse model

MMTV-PyMT female mice bearing primary tumors with an average volume of 400 mm^3 were divided into two groups and intraperitoneally injected with vehicle or CYD19 (30 mg/kg) for 25 consecutive days. Tumors were measured every 1 day using a caliper, and the volumes were calculated using the formula $\pi \times \text{length} \times \text{width}^2/6$. At the end of treatment point, mice were euthanized, and tumors, lungs, and key organs were dissected for further use.

Cloning, cell transfection, and virus production and infection

p3XFLAG-Snail-WT, p3XFLAG-Slug-WT, and pLKO.1-ms.p53-shRNA vectors were generated and used as described previously (*20, 21*). pET23a(+)-His-Snail-WT, His-Snail-R174A, p3XFLAG-Snail-R174A, FLAG-Snail-K147R/K186R, pLKO.1-hu.p53-shRNA (targeting mRNA sequence from ATG, 176 to 196), pLKO.1-Snail-shRNA1 (468 to 486), pLKO.1-Snail-shRNA2 (1515 to 1533), pCDN3.1-GST-Snail-WT-GFP, and pCDN3.1-GST-Snail-R174A-GFP

vectors were generated by GenScript Biotech Inc. (Nanjing, China). HA-ubiquitin (#18712), GST-CBP-HAT (#21093), pLKO.1-TRC (#10879), psPAX2 (#12260), and pMD2.G (#12259) were purchased from Addgene. To produce pLKO.1 lentiviral particles, HEK293T cells were cotransfected with pLKO.1-shRNA, psPAX2, and pMD2.G at a ratio of 4:3:1 using Lipofectamine 2000 Reagent (Invitrogen, #11668027). Cells were fed with fresh medium 24 hours after transfection, and conditioned medium containing viral particles was harvested 48 and 72 hours after transfection. Viral particles were stored at −80°C for further use or immediately used. For lentiviral infection, target cells were incubated with a mixture of conditioned medium (containing viral particles) and culture medium at a ratio of 1:1 for 24 hours in the presence of polybrene (8 μg/ml; Sigma-Aldrich, #H9268). Cells were reinfected with viral particles for another 24 hours and harvested for further use. For adenoviral infection, cells were infected with complete medium supplemented with adeno-βGal or adeno-Cre viral particles for 24 hours, refed with fresh medium containing viral particles, and further cultured for another 24 hours. Cells were collected for further use.

Immunoblot, IP, and His pulldown assays

For immunoblot analysis, cells were lysed in RIPA lysis buffer (Thermo Fisher Scientific, #89901) supplemented with protease inhibitor cocktail (#87786), and total cell lysates were collected for further uses. In some experiments, nuclear and (or) cytoplasmic proteins were extracted using the NE-PER Nuclear and Cytoplasmic Extraction Reagents (Thermo Fisher Scientific, #78833) according to the manufacturer's instructions. The cell lysates were subjected to immunoblot assay using primary antibodies against Snail (#3895; 1:1000), Slug (#9585; 1:1000), Cyt-c (#4280; 1:1000), caspase 3 (#9665; 1:1000), caspase 9 (#9508; 1:1000), cleaved caspase 3 (#9661; 1:500), cleaved caspase 9 (#52873; 1:500), p53 (#2524; 1:1,000), Bax (#2772; 1:1000), Puma (#24633; 1:1000), pan-acetyl-Lys (pan-AcK; #9441; 1:500), CBP (#7389; 1:1000), p300 (#70088; 1:1000), ubiquitin (#3936; 1:1000), HDAC1 (#5356; 1:1000), vimentin (#5741; 1:1000), histone H3 (#4499; 1:2000), HA-tag (#3724S; 1:2000), β-tubulin (#2128; 1:2000) (all from Cell Signaling Technology), E-cadherin (BD Biosciences, #610181; 1:5000), p21 (#ab7903; 1: 200), MDM2 (#ab16895; 1:500), phospho-Ser/Thr (#ab17464; 1:1000) (all from Abcam), FLAG (#F3165; 1:1000), importin β (Thermo Fisher Scientific, #MA3-070), and β-actin (#A5316; 1:10,000) (both from Sigma-Aldrich), followed by incubation with appropriate horse-radish peroxidase (HRP)–conjugated secondary antibodies. Blots were detected by enhanced chemiluminescence (Thermo Fisher Scientific, #32106). For IP assay, cells were lysed in IP lysis buffer [50 mM tris-HCl, 150 mM NaCl, 1 mM EDTA, and 1% NP-40 (pH 7.4)] containing protease inhibitor cocktail for 20 min on ice. The cell lysates were sonicated, clarified, and incubated with antibodies against control immunoglobulin G, FLAG (1:100), Snail (1:100), HDAC1 (1:100), or p53 (1:100), followed by incubation with precleared Protein A/G agarose beads (Santa Cruz Biotechnology, #sc-2003). The immunocomplexes were subjected to immunoblot analysis using antibodies against ubiquitin, HA, pan-AcK, phospho-Ser/Thr, CBP, p300, FLAG, or p53. For His pulldown assay, GST-CBP-HAT, His-Snail-WT, and His-Snail-R174A mutant recombinant proteins were expressed and purified from *E. coli* (BL21). The bead-bound His-tagged proteins were preincubated with various concentrations of CYD19 for 15 min at 4°C on a rotator, and eluted GST-CBP-HAT protein was added to the reaction mixtures and incubated for another 2 hours.

The beads were collected, extensively washed, eluted, electrophoresed, and subjected to Coomassie staining. In some experiments, His-Snail-WT and His-Snail-R174A mutant recombinant proteins were immobilized to Ni-NTA agarose and incubated with whole lysates of HEK293T cells for 3 hours (*34*). After extensive washes, the bound proteins were eluted with SDS sample buffer, resolved by SDS–polyacrylamide gel electrophoresis, and analyzed by immunoblotting.

Reverse transcription quantitative polymerase chain reaction analysis

Total RNAs were extracted and reversely transcribed using TRIzol reagent (Invitrogen, #15596018) and the PrimeScript RT reagent kit (Takara, #RR037A), respectively, according to the manufacturers' instructions. Quantitative polymerase chain reaction (qPCR) was performed on an Applied Biosystems QuantStudio 3 qPCR (Thermo Fisher Scientific) using the SYBR Green PCR Master Mix (Takara, #RR820A), and relative mRNA expressions were normalized to glyceraldehyde-3-phosphate dehydrogenase (GAPDH). qPCR primers for amplifying the indicated genes are used as follows: *GAPDH*, 5′-CACCGTCAAGGCTGAGAACGG-3′/5′-GACTCCAC-GACGTACTCAGCC-3′; *Gapdh*, 5′-CCCTGGCCAAGGTCATC-CATG-3′/5′-TGATGTTCTGGGCAGCCCCAC-3′; *SNAI1*, 5′-TCGGAAGCCTAACTACAGCGA-3′/5′-AGATGAGCATTGG-CAG CGAG-3′; *Snai1*, 5′-AAGATGCACATCCGAAGC-3′/5′-ATCTCTTCACATCCGAGTGG-3′; *TP53*, 5′-GTTCCGA-GAGCTGAATGAGG-3′/5′-TCTGAGTCAGGCCCTTCTGT-3′; *Trp53*, 5′-AGCTCCCTCTGAGCCAGGAGA-3′/5′-TCCTCAA-CATCCTGGGGCAGC-3′; *CDKN1A*, 5′-TCTTGTACCCTTGTG-CCTCG-3′/5′-GTTCCTGTGGGCGGATTAGG-3′; *Cdkn1a*, 5′-TG-CCGTTGTCTCTTCGGTCCC-3′/5′-TAGACCTTGGGCAGC-CCTAGG-3′; *MDM2*, 5′-GTGAATCTACAGGGACGCCATC-3′/5′-CTGATCCAACCAATCACCTGA A-3′; *Mdm2*, 5′-CGCT-GAGTGAGAGCAGACGTC-3′/5′-GCTCCCCAGGTAGCT-CATCTG-3′; *CDH1*, 5′-GTCAGTTCAGACTCCAGCCCG-3′/5′-CGTGTAGCTCTCGGCGTCAA-3′; *Cdh1*, 5′-GAAGTCCATGGG GCACCACCA-3′/5′-CTGAGACCTGGGTACACGCTG-3′; *CDH2*, 5′-CGACCCAAACAGCAACGACGC-3′/5′-CGGGTGCT-GAATTCCCTTGGC-3′; *Cdh2*, 5′-TGTGCACGAAGGACAGC-CCCT-3′/5′-CCTGCTCTGCAGTGAGAGGGA-3′; *VIM*, 5′-GC-CCTAGACGAACTGGGTC-3′/5′-GGCTGCAACTGCCTAAT-GAG-3′; *Vim*, 5′-AGCGTGGCTGCCAAGAACCTC-3′/5′-GCAG GGCATCGTGTTCCGGT-3′; *FN1*, 5′-CATCCCTGACCTGCTT CCTGG-3′/5′-CTGTACCCTGTGATGGGAGCC-3′; *Fn1*, 5′-GG-GTGACACTTATGAGCGCCC-3′/5′-GACTGACCCCCTTCAT-GGCAG-3′; *ERCC1*, 5′-GCATCATTGTGAGCCCTCGGC-3′/5′-GTGCAGGTTGTGGTAGCGGAG-3′; *Ercc1*, 5′-CCACAACCT CCATCCAGACTA-3′/5′-GCTTCTGCT CATACGCCTTGTA-3′; *CCL2*, 5′-AGTCTCTGCCGCCCTTCTGTG-3′/5′-CGCGAG-CCTCTGCACTGAGAT-3′; *Ccl2*, 5′-CTGTCATGCTTCTGGG-CCTGC-3′/5′-CAGC AGGTGAGTGGGGCGTTA-3′; *CCL5*, 5′-CAGCCCTCGCTGTCATCCTCA-3′/5′-GTGGGCGGG-CAATGTAGGCAA-3′; *Ccl5*, 5′-AGCAATGACAGGGAAGC-TATAC-3′/5′-AGGACTCTGAGACAGCACAT-3′; *TNFA*, 5′-GA TTCTGAGCAAAATAGCCAGCA-3′/5′-GGCTTCCT TCTTGTTGTGTGT-3′; *Tnfa*, 5′-CCCTCACACTCAGAT-CATCTTCT-3′/5′-GCTACGACGACGTGGGCTACA-3′; *IL8*, 5′-ACTGAGAGTGATTGAGAGTGGAC-3′/5′-AACCCTCTGCAC-CCAGTTTTC-3′; and *Il8*, 5′-TGTGAGGCTGCAGTTCTGG-CAAG-3′/5′-GGGTGGAAAGGTGTGGAATGCGT-3′. The specificity

of the PCR amplification was validated by the presence of a single peak in the melting curve analyses.

Histological, immunocytochemical, and immunohistochemical analyses

For histological assays, tumor and normal tissues were fixed in 4% PFA and embedded in paraffin. The embedded tissues were sectioned at 5 μm, deparaffinized, and subjected to hematoxylin and eosin (H&E) staining according to the manufacturer's instructions. For immuno-cytochemical analysis, cells were grown on chamber slides, fixed with 4% PFA, and incubated with primary antibodies against E-cadherin (1:1000), vimentin (1:200), Snail (1:200), or p53 (1:200), followed by incubation with goat anti-mouse and anti-rabbit Alexa secondary antibodies (all from Thermo Fisher Scientific, 1:300). Cells were then counter stained with 4it6-diamidino-2-phenylindole (DAPI), and images were acquired on a Zeiss LSM 800 microscope. For immuno-histochemical analysis, deparaffinized sections were rehydrated and subjected to antigen heat retrieval with citric acid–based Antigen Unmasking Solution (pH 6.0; Vector Laboratories, #H-3300). The sections were incubated in 0.3% H_2O_2 (in PBS) and then in blocking buffer (5% goat serum in PBS). The sections were then incubated in blocking buffer containing primary antibodies against Ki67 (Abcam, #ab15580; 1:1000), cleaved caspase 3 (1:100), phospho–histone H3 (Cell Signaling Technology, #9849; 1:200), and Snail (1:100), followed by incubation with biotinylated goat anti-mouse (Vector Laboratories, #BA-9200; 1:200) and goat anti-rabbit (Vector Laboratories, #BA-1000; 1:200) secondary antibodies. Standard avidin-biotin complex (ABC) kit (Vector Laboratories, #PK-6101) and 3,3-diaminobenzidine (DAB) HRP Substrate Kit (Vector Laboratories, #SK-4105) were used for the detection of HRP activity. Slides were counterstained with hematoxylin, dehydrated, and mounted. For immunofluorescence analysis, rehydrated tissues were incubated in blocking buffer containing primary antibodies against E-cadherin (1:400), vimentin (1:200), F4/80 (Thermo Fisher Scientific, #14-4801-81; 1:100), CD31 (Dianova, #DIA310; 1:100), or p53 (1:800), followed by incubation with goat anti-mouse, anti-rabbit, and anti-rat Alexa Fluor secondary antibodies (all from Thermo Fisher Scientific; 1:300). The sections were then counter stained with DAPI, and images were acquired on a Zeiss LSM 800 microscope.

Statistical analysis

Data were presented as means ± SD. Statistical analysis was carried out as described in each corresponding figure legend, and sample size were shown in each figure legend.

Differences were evaluated by Mann-Whitney U test, unpaired two-sided Student's t test, or one-way analysis of variance (ANOVA) with Tukey's post hoc test. $P < 0.05$ was considered statistically significant.

SUPPLEMENTARY MATERIALS

REFERENCES AND NOTES

1. P. Mehlen, A. Puisieux, Metastasis: A question of life or death. *Nat. Rev. Cancer* **6**, 449–458 (2006).
2. S. Valastyan, R. A. Weinberg, Tumor metastasis: Molecular insights and evolving paradigms. *Cell* **147**, 275–292 (2011).
3. L. J. Van't Veer, B. Weigelt, Road map to metastasis. *Nat. Med.* **9**, 999–1000 (2003).
4. L. Wan, K. Pantel, Y. Kang, Tumor metastasis: Moving new biological insights into the clinic. *Nat. Med.* **19**, 1450–1464 (2013).
5. J. P. Thiery, Epithelial–mesenchymal transitions in tumour progression. *Nat. Rev. Cancer* **2**, 442–454 (2002).
6. J. P. Thiery, H. Acloque, R. Y. Huang, M. A. Nieto, Epithelial-mesenchymal transitions in development and disease. *Cell* **139**, 871–890 (2009).
7. M. A. Nieto, The ins and outs of the epithelial to mesenchymal transition in health and disease. *Annu. Rev. Cell Dev. Biol.* **27**, 347–376 (2011).
8. B. De Craene, G. Berx, Regulatory networks defining EMT during cancer initiation and progression. *Nat. Rev. Cancer* **13**, 97–110 (2013).
9. S. A. Mani, W. Guo, M. J. Liao, E. N. Eaton, A. Ayyanan, A. Y. Zhou, M. Brooks, F. Reinhard, C. C. Zhang, M. Shipitsin, L. L. Campbell, K. Polyak, C. Brisken, J. Yang, R. A. Weinberg, The epithelial-mesenchymal transition generates cells with properties of stem cells. *Cell* **133**, 704–715 (2008).
10. D. Hanahan, R. A. Weinberg, Hallmarks of cancer: The next generation. *Cell* **144**, 646–674 (2011).
11. P. B. Gupta, T. T. Onder, G. Jiang, K. Tao, C. Kuperwasser, R. A. Weinberg, E. S. Lander, Identification of selective inhibitors of cancer stem cells by high-throughput screening. *Cell* **138**, 645–659 (2009).
12. D. R. Pattabiraman, B. Bierie, K. I. Kober, P. Thiru, J. A. Krall, C. Zill, F. Reinhardt, W. L. Tam, R. A. Weinberg, Activation of PKA leads to mesenchymal-to-epithelial transition and loss of tumor-initiating ability. *Science* **351**, aad3680 (2016).
13. E. Batlle, E. Sancho, C. Francí, D. Domínguez, M. Monfar, J. Baulida, A. García De Herreros, The transcription factor Snail is a repressor of E-cadherin gene expression in epithelial tumour cells. *Nat. Cell Biol.* **2**, 84–89 (2000).
14. A. Cano, M. A. Perez-Moreno, I. Locascio, M. J. Blanco, M. G. del Barrio, F. Portillo, M. A. Nieto, The transcription factor Snail controls epithelial–mesenchymal transitions by repressing E-cadherin expression. *Nat. Cell Biol.* **2**, 76–83 (2000).
15. M. A. Nieto, Epithelial plasticity: A common theme in embryonic and cancer cells. *Science* **342**, 1234850 (2013).
16. W. L. Tam, R. A. Weinberg, The epigenetics of epithelial-mesenchymal plasticity in cancer. *Nat. Med.* **19**, 1438–1449 (2013).
17. C. Kudo-Saito, H. Shirako, T. Takeuchi, Y. Kawakami, Cancer metastasis is accelerated through immunosuppression during Snail-induced EMT of cancer cells. *Cancer Cell* **15**, 195–206 (2009).
18. D. S. Hsu, H. J. Wang, S. K. Tai, C. H. Chou, C. H. Hsieh, P. H. Chiu, N. J. Chen, M. H. Yang, Acetylation of Snail modulates the cytokinome of cancer cells to enhance the recruitment of macrophages. *Cancer Cell* **26**, 534–548 (2014).
19. M. Kajita, K. McClinic, P. A. Wade, Aberrant expression of the transcription factors Snail and Slug alters the response to genotoxic stress. *Mol. Cell. Biol.* **24**, 7559–7566 (2004).
20. T. Ni, X.-Y. Li, N. Lu, T. An, Z.-P. Liu, R. Fu, W.-C. Lv, Y.-W. Zhang, X.-J. Xu, R. Grant Rowe, Y.-S. Lin, A. Scherer, T. Feinberg, X.-Q. Zheng, B.-A. Chen, X. S. Liu, Q.-L. Guo, Z.-Q. Wu, S. J. Weiss, Snail1-dependent p53 repression regulates expansion and activity of tumour-initiating cells in breast cancer. *Nat. Cell Biol.* **18**, 1221–1232 (2016).
21. Z.-Q. Wu, X.-Y. Li, C. Y. Hu, M. Ford, C. G. Kleer, S. J. Weiss, Canonical Wnt signaling regulates Slug activity and links epithelial-mesenchymal transition with epigenetic breast cancer 1, early onset (BRCA1) repression. *Proc. Natl. Acad. Sci. U.S.A.* **109**, 16654–16659 (2012).
22. S. Elloul, M. B. Elstrand, J. M. Nesland, C. G. Tropé, G. Kvalheim, I. Goldberg, R. Reich, B. Davidson, Snail, Slug, and Smad-interacting protein 1 as novel parameters of disease aggressiveness in metastatic ovarian and breast carcinoma. *Cancer* **103**, 1631–1643 (2005).
23. J. Geradts, A. G. de Herreros, Z. Su, J. Burchette, G. Broadwater, R. E. Bachelder, Nuclear Snail1 and nuclear ZEB1 protein expression in invasive and intraductal human breast carcinomas. *Hum. Pathol.* **42**, 1125–1131 (2011).
24. T. Imai, A. Horiuchi, C. Wang, K. Oka, S. Ohira, T. Nikaido, I. Konishi, Hypoxia attenuates the expression of E-cadherin via up-regulation of SNAIL in ovarian carcinoma cells. *Am. J. Pathol.* **163**, 1437–1447 (2003).
25. B. P. Zhou, J. Deng, W. Xia, J. Xu, Y. M. Li, M. Gunduz, M. C. Hung, Dual regulation of Snail by GSK-3β–mediated phosphorylation in control of epithelial-mesenchymal transition. *Nat. Cell Biol.* **6**, 931–940 (2004).
26. J. I. Yook, X. Y. Li, I. Ota, E. R. Fearon, S. J. Weiss, Wnt-dependent regulation of the E-cadherin repressor Snail. *J. Biol. Chem.* **280**, 11740–11748 (2005).
27. Y. Wu, J. Deng, P. G. Rychahou, S. Qiu, B. M. Evers, B. P. Zhou, Stabilization of Snail by NF-κB is required for inflammation-induced cell migration and invasion. *Cancer Cell* **15**, 416–428 (2009).
28. H. Zheng, M. Shen, L. Y. Zha, W. Li, Y. Wei, M. A. Blanco, G. Ren, T. Zhou, P. Storz, H. Y. Wang, Y. Kang, PKD1 phosphorylation-dependent degradation of Snail by SCF-FBXO11 regulates epithelial-mesenchymal transition and metastasis. *Cancer Cell* **26**, 358–373 (2014).
29. Y. Jin, A. K. Shenoy, S. Doernberg, H. Chen, H. Luo, H. Shen, T. Lin, M. Tarrash, Q. Cai, X. Hu, R. Fiske, T. Chen, L. Wu, K. A. Mohammed, V. Rottiers, S. S. Lee, J. Lu, FBXO11 promotes

ubiquitination of the Snail family of transcription factors in cancer progression and epidermal development. *Cancer Lett.* **362**, 70–82 (2015).

30. R. Viñas-Castells, M. Beltran, G. Valls, I. Gómez, J. M. García, B. Montserrat-Sentís, J. Baulida, F. Bonilla, A. G. de Herreros, V. M. Díaz, The hypoxia-controlled FBXL14 ubiquitin ligase targets SNAIL1 for proteasome degradation. *J. Biol. Chem.* **285**, 3794–3805 (2010).

31. R. Lander, K. Nordin, C. LaBonne, The F-box protein Ppa is a common regulator of core EMT factors Twist, Snail, Slug, and Sip1. *J. Cell Biol.* **194**, 17–25 (2011).

32. S. Choi, E. Yamashita, N. Yasuhara, J. Song, S. Y. Son, Y. H. Won, H. R. Hong, Y. S. Shin, T. Sekimoto, I. Y. Park, Y. Yoneda, S. J. Lee, Structural basis for the selective nuclear import of the C2H2 zinc-finger protein Snail by importin β. *Acta Crystallogr. D Biol. Crystallogr.* **70**, 1050–1060 (2014).

33. M. A. Nieto, A. Cano, The epithelial-mesenchymal transition under control: Global programs to regulate epithelial plasticity. *Semin. Cancer Biol.* **22**, 361–368 (2012).

34. J. M. Mingot, S. Vega, B. Maestro, J. M. Sanz, M. A. Nieto, Characterization of Snail nuclear import pathways as representatives of C_2H_2 zinc finger transcription factors. *J. Cell Sci.* **122**, 1452–1460 (2009).

35. H. Yamasaki, T. Sekimoto, T. Ohkubo, T. Douchi, Y. Nagata, M. Ozawa, Y. Yoneda, Zinc finger domain of Snail functions as a nuclear localization signal for importin β-mediated nuclear import. *Genes Cells* **10**, 455–464 (2005).

36. D. S. Hsu, H. Y. Lan, C. H. Huang, S. K. Tai, S. Y. Chang, T. L. Tsai, C. C. Chang, C. H. Tzeng, K. J. Wu, J. Y. Kao, M. H. Yang, Regulation of excision repair cross-complementation group 1 by Snail contributes to cisplatin resistance in head and neck cancer. *Clin. Cancer Res.* **16**, 4561–4571 (2010).

37. W. L. Huang, M. H. Yang, M. L. Tsai, H. Y. Lan, S. H. Su, S. C. Chang, H. W. Teng, S. H. Yang, Y. T. Lan, S. H. Chiou, H. W. Wang, The Snail-IL8 axis engenders stemness and tumorigenic characteristics in human colorectal carcinoma. *Gastroenterology* **141**, 279–291 (2011).

38. L. Wan, X. Lu, S. Yuan, Y. Wei, F. Guo, M. Shen, R. Chakrabarti, Y. Hua, H. A. Smith, M. A. Blanco, M. Chekmareva, H. Wu, R. T. Bronson, B. G. Haffty, Y. Xing, Y. Kang, MTDH-SND1 interaction is crucial for expansion and activity of tumor-initiating cells in diverse oncogene- and carcinogen-induced mammary tumors. *Cancer Cell* **26**, 92–105 (2014).

39. Y. Tang, W. Zhao, Y. Chen, Y. Zhao, W. Gu, Acetylation is indispensable for p53 activation. *Cell* **133**, 612–626 (2008).

40. E. Y. Lin, J. G. Jones, P. Li, L. Zhu, K. D. Whitney, W. J. Muller, J. W. Pollard, Progression to malignancy in the polyoma middle T oncoprotein mouse breast cancer model provides a reliable model for human diseases. *Am. J. Pathol.* **163**, 2113–2126 (2003).

41. C. Dong, T. Yuan, Y. Wu, Y. Wang, T. W. M. Fan, S. Miriyala, Y. Lin, J. Yao, J. Shi, T. Kang, P. Lorkiewicz, D. St. Clair, M. C. Hung, B. M. Evers, B. P. Zhou, Loss of FBP1 by Snail-mediated repression provides metabolic advantages in basal-like breast cancer. *Cancer Cell* **23**, 316–331 (2013).

42. S. E. Moody, D. Perez, T. C. Pan, C. J. Sarkisian, C. P. Portocarrero, C. J. Sterner, K. L. Notorfrancesco, R. D. Cardiff, L. A. Chodosh, The transcriptional repressor Snail promotes mammary tumor recurrence. *Cancer Cell* **8**, 197–209 (2005).

43. Y. Wu, Y. Wang, Y. Lin, Y. Liu, Y. Wang, J. Jia, P. Singh, Y. I. Chi, C. Wang, C. Dong, W. Li, M. Tao, D. Napier, Q. Shi, J. Deng, B. M. Evers, B. P. Zhou, Dub3 inhibition suppresses breast cancer invasion and metastasis by promoting Snail1 degradation. *Nat. Commun.* **8**, 14228–14243 (2017).

44. Z.-Q. Wu, R. G. Rowe, K. C. Lim, Y.-S. Lin, A. Willis, Y. Tang, X.-Y. Li, J. E. Nor, I. Maillard, S. J. Weiss, A Snail1/Notch1 signalling axis controls embryonic vascular development. *Nat. Commun.* **5**, 3998–4012 (2014).

45. E. A. Carver, R. Jiang, Y. Lan, K. F. Oram, T. Gridley, The mouse Snail gene encodes a key regulator of the epithelial-mesenchymal transition. *Mol. Cell. Biol.* **21**, 8184–8188 (2001).

46. M. Olivier, M. Hollstein, P. Hainaut, TP53 mutations in human cancers: Origins, consequences, and clinical use. *Cold Spring Harb. Perspect. Biol.* **2**, a001008 (2010).

47. S. Piccinin, E. Tonin, S. Sessa, S. Demontis, S. Rossi, L. Pecciarini, L. Zanatta, F. Pivetta, A. Grizzo, M. Sonego, C. Rosano, A. P. Dei Tos, C. Doglioni, R. Maestro, A "twist box" code of p53 inactivation: Twist box: p53 interaction promotes p53 degradation. *Cancer Cell* **22**, 404–415 (2012).

48. B. Beck, G. Lapouge, S. Rorive, B. Drogat, K. Desaedelaere, S. Delafaille, C. Dubois, I. Salmon, K. Willekens, J. C. Marine, C. Blanpain, Different levels of Twist1 regulate skin tumor initiation, stemness, and progression. *Cell Stem Cell* **16**, 67–79 (2015).